IEEE Access
Multidisciplinary | Rapid Review | Open Access Journal

Received May 15, 2020, accepted May 23, 2020, date of publication May 29, 2020, date of current version June 11, 2020.

Digital Object Identifier 10.1109/ACCESS.2020.2997987

Influence of Coal Gangue Volume Mixing Ratio on the System Contact Response When Multiple Coal Gangue Particles Impacting the Metal Plate and the Study of Coal Gangue Mixing Ratio Recognition Based on the Metal Plate Contact Response and the Multi-Information Fusion

YANG YANG[1], QINGLIANG ZENG[1,2], LIRONG WAN[1], AND GUANGJUN YIN[1]

[1]College of Mechanical and Electronic Engineering, Shandong University of Science and Technology, Qingdao 266590, China
[2]College of Information Science and Engineering, Shandong Normal University, Jinan 250358, China

Corresponding author: Lirong Wan (lirong.wan@sdust.edu.cn)

This work was supported in part by the National Natural Science Fund of China under Grant 51674155, in part by the National Natural Science Fund of China under Grant 51974170, in part by the Innovative Team Development Project of Ministry of Education under Grant IRT_16R45, and in part by the Special Funds for Climbing Project of Taishan Scholars.

ABSTRACT In order to clearly grasp the influence rules of the coal gangue volume mixture ratio on the system contact response, and finally realize the coal gangue mixing ratio recognition according to the contact response differences, on the basis of the Hertz contact theory and Flores nonlinear spring-damping contact theory, this paper proposed and established the theoretical model when multiple coal gangue particles elastic impacting the metal plate for the first time simultaneously in an undisturbed way with the consideration of the particles micro-compression, the macro-deflection of the metal plate and the functional transformation of the system. To further study the system response, the simulation when multiple coal gangue particles with the variable mixing ratio impacting the metal plate was carried out with consideration of the coal gangue brittleness and the elastic-plastic of metal plate. Then, broken response of coal gangue particles and the contact response of the metal plate under the different coal gangue mixing ratios were studied. After that, EMD decomposition and time-frequency domain parameters calculation were conducted for the vibration acceleration signal of the metal plate, and the influence law of gangue mixing ratio on the vibration acceleration signal time-frequency domain parameters of the metal plate was obtained. Finally, in line accordance with the self-proposed data standardization processing method, Kalman filtering, multi-information fusion method as well as the simulation data, the recognition of coal gangue mixture ratio based on the vibration acceleration signal multi-time-frequency domain parameter fusion and the recognition of coal gangue mixture ratio based on the metal plate multi-response information fusion were marched respectively, and the coal gangue mixture ratio multi-dimension recognition strategy based on Kalman filter and the energy fusion is proposed. The research results show that the proposed recognition method can greatly improve the recognition rate and the applicability of the identification strategy.

INDEX TERMS Impact, contact response, gangue mixing ratio recognition, Kalman filter, signal, multi-information fusion.

I. INTRODUCTION

Coal is the important source of energy and fuel, which it's mining technology is closely related to the social and economic development. Top caving coal mining is the principal method of thick seam mining. In order to improve the coal mining efficiency, the development and research of automatic coal mining technology are very important. During the mining process of top coal caving [1]–[4], the hydraulic support is in close interaction with the roof, floor, surrounding

The associate editor coordinating the review of this manuscript and approving it for publication was Hamid Mohammad-Sedighi.

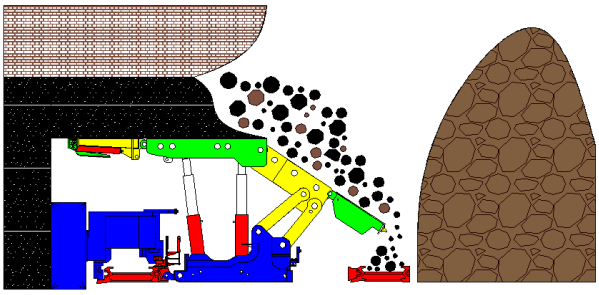

FIGURE 1. Top coal caving.

rock and a large number of coal gangue particles, as shown in Figure 1, together with the shearer and scraper, they constitutes a fully mechanized caving mining process which is composed of mining, supporting and transportation in the underground coal mining space [5]. In this process, there are collisions between coal and gangue, single particle of coal gangue and the metal plate of the hydraulic support, multiple particles of coal gangue and the metal plate of the hydraulic support, coal gangue particles group and the metal plate of the hydraulic support, as shown in Figure 2. Yang *et al.* [6], [7] studied the system contact dynamic response when a single particle elastic impacting the metal plate or elastic half-space by theoretical and simulation methods, and used the research idea of breaking up the whole into parts and the point-to-surface research thinking [8] to disassemble the complex top coal gangue identification problem and completed the coal gangue identification when the single coal gangue impacts the center position of the metal plate. Zeng *et al.* [9] analyzed the dynamic process and impact response of the metal plate after the impact of the single particle coal gangue. Xie and Zhao [10], Yang *et al.* [11], Yang *et al.* [12], Wang *et al.* [13], Zhang *et al.* [2], Zhang *et al.* [14], Song and Konietzky constructed a slip model of coal gangue particles group along the hydraulic support by discrete element method, and studied the release law of the top coal, caving property, top coal loss pattern and so on. Zhang *et al.* [16], Wang *et al.* [17], Zhang *et al.* [3], and Zhang *et al.* [18] carried out the drop test of coal gangue particles along the hydraulic support or the 3D test device, conducted the simulation of top coal releasing process, and investigated the loose top-coal drawing law of longwall top-coal caving mining technology and arching phenomenon as well as the top coal recovery rate. These studies provide theoretical, simulation and experimental methods for the study of the impact contact and interaction between the single coal gangue or coal gangue particles group and the hydraulic supports or metal plates. However, due to the lack of the concept of the impact or contact problem between the multiple coal gangue particles and the hydraulic support in the earlier stage, and because of the influence and limitation of multiple coal gangue particles number, shape, arrangement of the and its contact mode with the hydraulic support, the interaction research between multiple coal gangue particles and the hydraulic support in the top coal caving process is still in the blank at present.

The accurate identification of multiple coal gangue particles mixing ratio in the top coal caving process is of great significance in the identification of the coal gangue particles group mixing ratio. It is the premise and guarantee for the accurate realization of the interface identification of top coal caving. It is also the key problem that top coal caving unmanned automation must solve. Zhang and Liu [19] used the natural gamma ray technology to identify the coal gangue during top coal caving. Hou [20] proposed a method for identifying coal gangue by combining image feature extraction with an artificial neural network. Based on the PQN-NN and the DS theory, Si *et al.* [21] put forward a multi-sensor data fusion identification method for the shearer cutting state identification. Song *et al.* [22], [23] designed a vibration and sound signal acquisition model, constructed a new coal rock identification discriminant analysis framework, and proposed a new multi-class feature selection method for different proportions of coal gangue identification. Sun and Su [24] proposed a coal gangue interface identification method based on the coal gangue texture feature differences and the digital image analysis techniques. Tripathy and Reddy [25] proposed an ore sorting model based on visual and color texture feature analysis, and used multi-spectral and joint color texture features to separate limestone and coal. Liu *et al.* [26] identified coal gangue by analyzing the vibration signal of the tail beam of the hydraulic support. Dou *et al.* [27] applied image analysis and Relief-SVM method to classify and identify coal gangue with different surface conditions. Wang *et al.* [28] combined the improved particle swarm optimization algorithm with the wavelet neural network to identify the cutting load of the shearer. Cong *et al.* [29] performed EMD decomposition and kurtosis filtering on the vibration signal of the hydraulic support tail beam to realize the coal gangue interface identification. Wang [30], Wang *et al.* [31] used electromagnetic wave technology and terahertz time-domain spectroscopy to identify coal and rock. Huang [32] identified the coal rock interface during the cutting process of the shearer by clustering image recognition technology. Hua *et al.* [33] proposed the coal gangue identification method by the combination of the dimensionless parameters and support vector machine method in top coal caving. The above proposed coal gangue identification method and identify research results provided a research basis and reference for the identification of multiple coal gangue particles mixing ratio. However, due to the lack of the theoretical research on the contact response between multi-particles and the metal plate in the early stage, and the restriction of various conditions such as the inter particles disturbance behavior and the superposition of the metal plate contact response after multi-particle impact, the difficulty of the research when multi-particles impacting the hydraulic support or the metal plate is greatly increased, and the generation, evolution and propagation of signals during the impact contact between multi-particles and the metal plate became difficult to clearly understand. Mastering the impact contact response law between multi-particles and the metal plate is the premise of

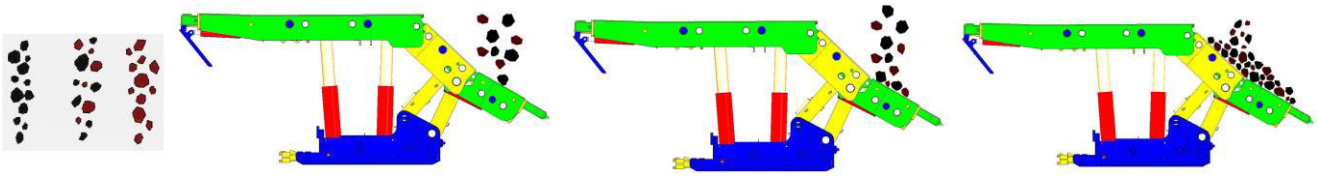

FIGURE 2. Collision contact between the coal gangue and the hydraulic support in top coal caving.

realizing the coal gangue proportion identification according to the contact response of multiple coal gangue particles and the metal plate, as a result, it has seriously restricted the development of multiple coal gangue particles mixing ratio recognition technology based on data analysis.

Based on the previous research results and the research shortages of the single particle, group particle and coal gangue recognition, in order to comprehensively grasp the contact response law when multiple coal gangue particles impacting the metal plate, and finally realize the identification of multiple coal gangue particles mixing ratio, this paper referring to the research method of the previous contact problem [34]–[40], on the basis of the Hertz contact theory and the Flores contact model, considering the medium compression and the deformation of the metal plate, proposes the theoretical model when the multiple coal gangue particles simultaneously undisturbed elastic impacting the metal plate in the first time under four different working conditions. Furthermore, a simulation model when the multiple coal gangue particles with the variable mixing ratio impacting the equal center distance of the metal plate is constructed, and the broken response of the particles and the contact response of the metal plate are obtained. In line accordance with the simulation data, the EMD decomposition and time-frequency domain parameters calculation are conducted to the vibration acceleration signal of the metal plate, and the variation law of the time-frequency parameters of the metal plate vibration acceleration signal under different mixing ratios is obtained. To realize the coal gangue mixing ratio identification, the simulation data is standardized, Kalman filtering and multi-information fusion and other further processing, the optimal data fusion method is determined by the coal gangue mixing ratio identification based on the vibration acceleration signal multi-time-frequency domain parameters fusion and the coal gangue mixing ratio identification based on the metal plate multi-response information fusion, and the multi-dimensional accurate identification strategy of coal gangue mixing ratio is finally proposed.

The contributions of the paper include:

- This paper proposed and established the theoretical model when multiple coal gangue particles elastic impacting the metal plate for the first time simultaneously in an undisturbed way.
- Coal gangue mixture ratio multi-dimension recognition strategy with high precision, high reliability and strong applicability based on Kalman filter and the energy fusion is proposed in this paper.

The remainder of the paper is organized as follows: Section 2 establishes a theoretical model when multiple coal gangue particles simultaneously undisturbed elastic impacting the metal plate in the first time, and the elastic contact force of the system is analyzed. Section 3 constructs a simulation model when the multiple coal gangue particles with the variable mixing ratio impacting the equal center distance of the metal plate, and analyzes the influence of the gangue mixing ratio on the particle broken response and the metal plate contact response. Section 4 carries out the EMD decomposition and time-frequency domain analysis to the vibration acceleration signals of the metal plate. Section 5 conducts the standardized processing and the Kalman filter to the different contact response signals of the metal plate, completes the coal gangue mixture ratio recognition based on the vibration acceleration signal multi-time-frequency domain parameter fusion and the recognition based on the metal plate multi-response information fusion, and proposes the optimal coal gangue mixing ratio recognition strategy based on the information fusion and the multi-dimension identification. Section 6 shows some related work and our conclusions.

II. THEORETICAL MODEL OF MULTIPLE COAL GANGUE PARTICLES IMPACTING THE METAL PLATE

A. CONTACT FORCE MODEL

Hertz proposed the widely accepted interface contact theory [41]–[43]:

$$P_{Her} = K \cdot \delta^{\frac{3}{2}} \tag{1}$$

$$K = \frac{4\sqrt{R}}{3} \cdot E \tag{2}$$

$$E = \frac{1-\mu_1^2}{E_1} + \frac{1-\mu_2^2}{E_2} \tag{3}$$

$$\frac{1}{R} = \frac{1}{R_1} + \frac{1}{R_2} \tag{4}$$

where P_{Her} is the Hertz contact force, K is the contact stiffness, δ is the contact deformation, R and E is the equivalent contact radius and elastic modulus respectively, E_1 and E_2 is the elastic modulus of two respectively contact body, μ_1 and μ_2 is the Poisson's ratio of two respectively contact body, and R_1 and R_2 is the radius of two respectively contact body.

Hertz contact theory takes into account the elastic contact of the objects and builds the foundation for subsequent contact theory. On this basis, Flores established a nonlinear spring-damped contact theory that considers both the system

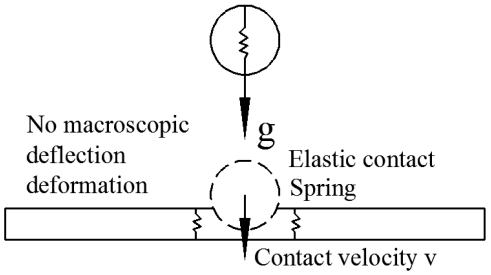

FIGURE 3. Complete Hertz contact state.

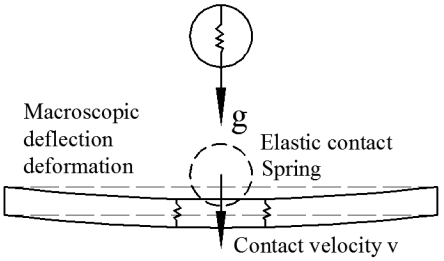

FIGURE 4. Hertz contact macroscopic deflection deformation state.

elastic force and the damping dissipation force [6], [44], [45]:

$$P_{Flor} = K \cdot \delta^n + D \cdot \dot{\delta} \tag{5}$$

where the contact damping $D = K \cdot \delta^n \cdot \frac{8(1-e)}{5e\dot{\delta}^{(-)}}$, P_{Flor} is the Flores contact force, nonlinear contact coefficient $n = 1.5$, $\dot{\delta}$ is the instantaneous velocity of the sphere and $\dot{\delta}^{(-)}$ is the initial velocity, e is the restitution coefficient.

B. FUNCTIONAL TRANSFORMATION OF THE SYSTEM DURING CONTACT

1) FUNCTIONAL TRANSFORMATION MODEL IN CONTACT PROCESS

During the contact of the particles with the metal plate, the compression deformation of the particles and the macroscopic deflection deformation of the metal plates are existed. If only the Hertz contact force during the contact process is considered, regardless of the damping force and the deformation of the metal plate, defined this condition as the complete Hertz contact state, as shown in Figure 3, the system energy conversion model can be expressed as:

$$\frac{1}{2}m \cdot v^2 = \int P_{Her} d\delta = \int K \cdot \delta^{\frac{3}{2}} d\delta \tag{6}$$

where m and$v$ is the mass and velocity of the particle.

Define $\delta_{\max -PH}$ is maximum complete Hertz deformation, the system functional relationship in the ultimate compression state system of the complete Hertz contact state is:

$$\frac{1}{2}m \cdot v^2 = \frac{2}{5}K \cdot \delta_{\max -PH}^{\frac{5}{2}} \tag{7}$$

According to this, the maximum compression deformation $\delta_{\max -PH}$ of the rock under the complete Hertz contact state and the system maximum contact force $P_{\max -PH}$ are obtained:

$$\delta_{\max -PH} = \left(\frac{5m \cdot v^2}{4K}\right)^{\frac{2}{5}} \tag{8}$$

$$P_{\max -PH} = K^{\frac{2}{5}} \left(\frac{5m \cdot v^2}{4}\right)^{\frac{3}{5}} \tag{9}$$

However, the metal plate may deform under force [46], [47]. Considering the Hertz contact force and the deflection of the metal plate during the contact process, as shown in Figure 4, defined this condition as the Hertz contact macroscopic deflection deformation state and $I_2 = \frac{Bh^3}{12}$. Under the Hertz contact force, the deflection equation of the metal plate ω_{HN} and the energy W_{JN} absorbed by the deflection of the metal plate are:

$$\omega_{HN} = \frac{P_{Her} \cdot y}{6E_2I_2L} \cdot x \cdot \left(L^2 - x^2 - y^2\right) \tag{10}$$

$$W_{JN-HN} = \frac{P_{Her}^2 \cdot y}{12E_2I_2L} \cdot x \cdot \left(L^2 - x^2 - y^2\right) \tag{11}$$

where L is the length of the metal plate, x is the distance from the left end of the metal plate to the impact point, y is the distance from the right end of the metal plate to the impact point. The system energy conversion model of the Hertz contact macroscopic deflection deformation state can be expressed as:

$$\frac{1}{2}m \cdot v^2 = \int P_{Her} d\delta + W_{JN-HN} = \int K \cdot \delta^{\frac{3}{2}} d\delta + \frac{K^2 \cdot \delta^3 \cdot y}{12E_2I_2L} \cdot x \cdot \left(L^2 - x^2 - y^2\right) \tag{12}$$

Then the expression of the maximum compression deformation $\delta_{\max -HN}$ of the rock under the Hertz contact macroscopic deflection state is:

$$\frac{1}{2}m \cdot v^2 = \frac{2}{5}K \cdot \delta_{\max -HN}^{\frac{5}{2}} + \frac{K^2 \cdot \delta_{\max -HN}^3 \cdot y \cdot x \cdot \left(L^2 - x^2 - y^2\right)}{12E_2I_2L} \tag{13}$$

Considering both the system elastic force and the damping dissipation force, regardless of the deflection of the metal plate, defined this condition as the complete Flores contact state, as shown in Figure 5, the system energy conversion model can be expressed as:

$$\frac{1}{2}m \cdot v^2 = \int P_{Flore} d\delta = \int \left(K \cdot \delta^n + K \cdot \delta^n \cdot \frac{8\,(1-e)}{5e\,\dot{\delta}^{(-)}} \cdot \dot{\delta}\right) d\delta \tag{14}$$

From reference [6] and [44], when the maximum deformation of the particle is $\delta_{\max}$:

$$\dot{\delta} = \dot{\delta}^{(-)} \sqrt{1 - \left(\frac{\delta}{\delta_{\max}}\right)^2} \tag{15}$$

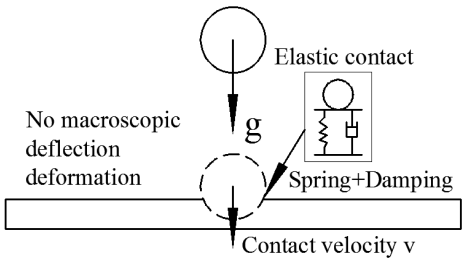

FIGURE 5. Complete Flores contact state.

Define $\delta_{\max -PF}$ is maximum complete Flores deformation, then the system functional relationship in the ultimate compression state of the complete Flores contact state is:

$$\frac{1}{2}m \cdot v^2 = \frac{2}{5}K \cdot \delta_{\max -PF}^{\frac{5}{2}} + \frac{8K\,(1-e)}{5e}\int_0^{\delta_{\max -PF}} \delta^n \cdot \sqrt{1-\left(\frac{\delta}{\delta_{\max -PF}}\right)^2}\,d\delta \quad (16)$$

Equation (16) is integrated according to the reference [6] and [48] and obtained that:

$$\frac{1}{2}m \cdot v^2 = \frac{2}{5}K \cdot \delta_{\max -PF}^{\frac{5}{2}} + \frac{8K\,(1-e)}{5e}\delta_{\max -PF}^{\frac{5}{2}}\int_0^1 z^{\frac{3}{2}} \cdot \sqrt{1-z^2}dx \quad (17)$$

where z is a variate, further calculate obtained that:

$$\frac{1}{2}m \cdot v^2 = \frac{2}{5e}K \cdot \delta_{\max -PF}^{\frac{5}{2}} \quad (18)$$

According to this, the maximum compression deformation $\delta_{\max -PF}$ of the complete Flores contact state and the system maximum contact force $P_{\max -PF}$ can be expressed respectively:

$$\delta_{\max -PF} = \left(\frac{5e \cdot m \cdot v^2}{4K}\right)^{\frac{2}{5}} \quad (19)$$

$$P_{\max -PF} = K^{\frac{2}{5}}\left(\frac{5e \cdot m \cdot v^2}{4}\right)^{\frac{3}{5}} \quad (20)$$

However, in the process of rock ball compression, the deflection deformation of the metal plate is often accompanied. Considering the Flores contact force during contact and the deformation of the metal plate, this condition is defined as the Flores contact macroscopic deflection state, as shown in Figure 6. Under the Flores contact force, the deflection equation of the metal plate ω_{FN} and the energy W_{JN} absorbed by the deflection of the metal plate are:

$$\omega_{FN} = \frac{P_{Flor} \cdot y}{6E_2I_2L} \cdot x \cdot \left(L^2 - x^2 - y^2\right) \quad (21)$$

$$W_{JN-FN} = \frac{P_{Flor}^2 \cdot y}{12E_2I_2L} \cdot x \cdot \left(L^2 - x^2 - y^2\right) \quad (22)$$

The system energy conversion model of the Flores contact macroscopic deflection deformation state can be expressed as Equation (23), as shown at the bottom of the next page.

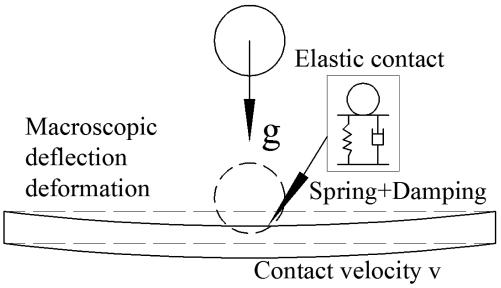

FIGURE 6. Flores contact macroscopic deflection state.

Then the system functional relationship in the ultimate compression state of the Flores contact macroscopic deflection deformation state is Equation (24), as shown at the bottom of the next page.

Combined with Equation (16), we get that Equation (25), as shown at the bottom of the next page, and finally obtain the Equation (26), as shown at the bottom of the next page.

2) SOLUTION OF THE SYSTEM FUNCTIONAL TRANSFORMATION MODEL WHEN THE DEFLECTION DEFORMATION OF THE METAL PLATE ABSORBED THE ENERGY

When considering the energy absorption of the metal plate, the system energy will be composed of the energy absorbed by the contact force and the energy absorbed by the bending deformation of the metal plate, as shown in Equation (13) and (26). In the equations, both $\delta^{\frac{5}{2}}$ and δ^3 are unknown high-order terms. According to the approximate analytical solution method of the high-order equations based on the recursive solution proposed in reference [6], the energy conversion model in the ultimate compression state of the Hertz contact macroscopic deflection state and the Flores contact macroscopic deflection state are solved. Equations (13) and (26) are equivalently converted to Equations (27) and (28), as shown at the bottom of the next page. Define γ is the Precision of $\delta_{\max}$, we can obtain the Equations (29), as shown at the bottom of the next page.

Simultaneously, the maximum contact force of the system is:

$$\begin{cases} P_{\max -HN-N} = K \cdot \delta_{\max -HN-N}^{\frac{3}{2}} \\ P_{\max -FN-N} = K \cdot \delta_{\max -FN-N}^{\frac{3}{2}} \end{cases} \quad (30)$$

C. THEORETICAL MODEL WHEN THE MULTIPLE COAL GANGUE PARTICLES UNDISTURBED IMPACTING THE METAL PLATE IN THE FIRST TIME

After multiple coal gangue particles vertically impact on the metal plate at a certain speed, the springback of the particles and their reciprocating collision with the metal plate occur. Contact behavior between the particles and the metal plate will trigger the compression of the rock ball, the bending deformation of the metal plate. And the impact position of the particle on the metal plate is not the center of the metal

plate, so that multiple reciprocating rebound velocity of the particles is offset from the vertical line, thereby generating the difficult-to-quantify contact behavior and even the disordered collisions between particles after the rebound. For quantitative analysis, only the once impact between coal gangue particles and the metal plate is considered here, and the influence of the contact behavior between the particles and the metal plate on the contact response between other particles and the metal plate is not considered. The equivalent elastic modulus when coal or gangue respectively impact contact with the metal plate is:

$$E_C = \frac{1-\mu_1^2}{E_{Coal}} + \frac{1-\mu_2^2}{E_{Metal}} \tag{31}$$

$$E_G = \frac{1-\mu_1^2}{E_{Gangue}} + \frac{1-\mu_2^2}{E_{Metal}} \tag{32}$$

Where E_{Coal}, E_{Gangue} and E_{Metal} is the elastic modulus of coal, gangue and the metal plate respectively. The contact stiffness when coal gangue impact is:

$$K_C = \frac{4\sqrt{R}}{3} \cdot E_C \tag{33}$$

$$K_G = \frac{4\sqrt{R}}{3} \cdot E_G \tag{34}$$

Substituting Eqs. (33) and (34) into Eqs. (8), (9), (19), (20), (28), and (30), respectively. Then the maximum rock ball compression deformation and the system maximum

$$\frac{1}{2}m \cdot v^2 = \int P_{Flor} d\delta + W_{JN-FN} = \int \left(K \cdot \delta^n + K \cdot \delta^n \cdot \frac{8\,(1-e)}{5e\overset{\bullet}{\delta}^{(-)}} \cdot \overset{\bullet}{\delta} \right) d\delta + \frac{\left(K \cdot \delta^n + D \cdot \overset{\bullet}{\delta} \right)^2 \cdot y}{12E_2I_2L} \cdot x \cdot \left(L^2 - x^2 - y^2 \right) \tag{23}$$

$$\frac{1}{2}m \cdot v^2 = \frac{2}{5e}K \cdot \delta_{\max -FN}^{\frac{5}{2}} + \frac{\left[K \cdot \delta^n + K \cdot \delta^n \cdot \frac{8(1-e)}{5e\overset{\bullet}{\delta}^{(-)}} \cdot \overset{\bullet}{\delta} \right]^2 \cdot y}{12E_2I_2L} \cdot x \cdot \left(L^2 - x^2 - y^2 \right) | \delta = \delta_{\max -FN} \tag{24}$$

$$\frac{1}{2}m \cdot v^2 = \frac{2}{5e}K \cdot \delta_{\max -FN}^{\frac{5}{2}} + \frac{\left[K \cdot \delta^n + K \cdot \delta^n \cdot \frac{8(1-e)}{5e} \cdot \sqrt{1 - \left(\frac{\delta}{\delta_{\max -FN}} \right)^2} \right]^2 \cdot y}{12E_2I_2L} \cdot x \cdot \left(L^2 - x^2 - y^2 \right) | \delta = \delta_{\max -FN} \tag{25}$$

$$\frac{1}{2}m \cdot v^2 = \frac{2}{5e}K \cdot \delta_{\max -FN}^{\frac{5}{2}} + \frac{K^2 \delta_{\max -FN}^3 \cdot y \cdot x \cdot \left(L^2 - x^2 - y^2 \right)}{12E_2I_2L} \tag{26}$$

$$\begin{cases} \delta_{\max -HN}^{\frac{5}{2}} = \dfrac{m \cdot v^2}{2\left[\frac{2K}{5} \cdot + \frac{K^2 \cdot \delta_{\max -HN}^{\frac{1}{2}} \cdot y \cdot x \cdot \left(L^2 - x^2 - y^2 \right)}{12E_2I_2L} \right]} \\ \delta_{\max -FN}^{\frac{5}{2}} = \dfrac{m \cdot v^2}{2\left[\frac{2K}{5e} \cdot + \frac{K^2 \cdot \delta_{\max -FN}^{\frac{1}{2}} \cdot y \cdot x \cdot \left(L^2 - x^2 - y^2 \right)}{12E_2I_2L} \right]} \end{cases} \tag{27}$$

$$\begin{cases} \delta_{\max -HN-N}^{\frac{5}{2}} = \left\{ \dfrac{m \cdot v^2}{2\left[\frac{2K}{5} \cdot + \frac{K^2 \cdot y \cdot x \cdot \left(L^2 - x^2 - y^2 \right)}{12E_2I_2L} \delta_{\max -HN(N-1)}^{\frac{1}{2}} \right]} \right\}^{\frac{2}{5}} \\ \delta_{\max -FN-N}^{\frac{5}{2}} = \left\{ \dfrac{m \cdot v^2}{2\left[\frac{2K}{5e} \cdot + \frac{K^2 \cdot y \cdot x \cdot \left(L^2 - x^2 - y^2 \right)}{12E_2I_2L} \delta_{\max -FN(N-1)}^{\frac{1}{2}} \right]} \right\}^{\frac{2}{5}} \end{cases} \tag{28}$$

$$\begin{cases} \dfrac{\left| \frac{2K}{5} \cdot \delta_{\max -HN-N}^{\frac{5}{2}} + \frac{K^2 \delta_{\max -HN-N}^3 \cdot y \cdot x \cdot \left(L^2 - x^2 - y^2 \right)}{12E_2I_2L} - \frac{1}{2}m \cdot v^2 \right|}{\frac{1}{2}m \cdot v^2} \le \gamma \\ \dfrac{\left| \frac{2K}{5e} \cdot \delta_{\max -FN-N}^{\frac{5}{2}} + \frac{K^2 \delta_{\max -FN-N}^3 \cdot y \cdot x \cdot \left(L^2 - x^2 - y^2 \right)}{12E_2I_2L} - \frac{1}{2}m \cdot v^2 \right|}{\frac{1}{2}m \cdot v^2} \le \gamma \end{cases} \tag{29}$$

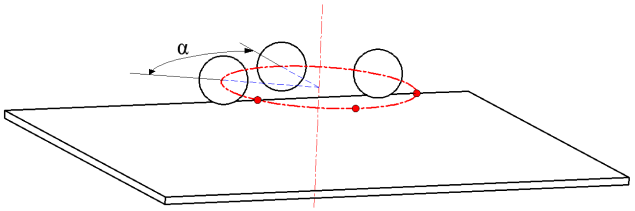

FIGURE 7. Particles equiangular arranged.

contact force when the coal gangue impact at optional position of the metal plate under the complete Hertz contact state, the Hertz contact macroscopic deflection deformation state, the complete Flores contact state, and the Flores contact macroscopic deflection deformation state can be obtained.

It is assumed that the particles equiangular (Angle α) arranged on a circle with the radius RR around the axis of the metal plate, as shown in Figure 7. The length, width and thickness of the metal plate are L_L, B_B, and H, respectively. And the center distances of the four support rods of the metal plate are respectively length L and width B, and the particle radius is R(to ensure that the particles are simultaneously in contact with the metal plate). The total number of particles is set to nn(nn is an even number and $nn \geq 2$), wherein the number of gangue is t($t \leq nn$), that is, i.e. the mixing ratio of gangue is $\frac{t}{nn} \times 100\%$, of which two particles (A, B) is located on the central axis of the metal plate, and the remaining particles are symmetrically arranged along the central axis. Defining coal as $j = 1$, gangue as $j = 2$, then the contact stiffness K_C and K_G can be written as K_j. Maximum compression deformation of the rock ball and maximum contact force when i^{th} particle ($1 \leq i \leq nn$) impacting the metal plate is shown in Equations (35) and (36), as shown at the bottom of this page.

When the multiple particles simultaneously elastically impact, the maximum total contact force is:

$$P_{T\max} = \sum_{1}^{nn} P_{\max -i} \tag{37}$$

$$\delta_{\max -i} = \begin{cases} \delta_{\max -PH-i} = \left(\dfrac{5m \cdot v^2}{4K_j}\right)^{\frac{2}{5}} \\ \delta_{\max -HN-N-i} = \left\{\dfrac{m \cdot v^2}{2\left[\dfrac{2K_j}{5} \cdot + \dfrac{K_j^2 \cdot y_i \cdot x_i \cdot \left(L^2 - x_i^2 - y_i^2\right)}{12E_2I_2L}\delta^{\frac{1}{2}}_{\max -HN(N-1)-i}\right]}\right\}^{\frac{2}{5}} \\ \delta_{\max -PF-i} = \left(\dfrac{5e \cdot m \cdot v^2}{4K_j}\right)^{\frac{2}{5}} \\ \delta_{\max -FN-N-i} = \left\{\dfrac{m \cdot v^2}{2\left[\dfrac{2K_j}{5e} \cdot + \dfrac{K_j^2 \cdot y_i \cdot x_i \cdot \left(L^2 - x_i^2 - y_i^2\right)}{12E_2I_2L}\delta^{\frac{1}{2}}_{\max -FN(N-1)-i}\right]}\right\}^{\frac{2}{5}} \end{cases} \tag{35}$$

$$P_{\max -i} = \begin{cases} P_{\max -PH-i} = K_j^{\frac{2}{5}} \cdot \left(\dfrac{5m \cdot v^2}{4}\right)^{\frac{3}{5}} \\ P_{\max -HN-N-i} = K_j^{\frac{2}{5}} \cdot \left\{\dfrac{m \cdot v^2}{2\left[\dfrac{2}{5} \cdot + \dfrac{K_j \cdot y_i \cdot x_i \cdot \left(L^2 - x_i^2 - y_i^2\right)}{12E_2I_2L}\delta^{\frac{1}{2}}_{\max -HN(N-1)-i}\right]}\right\}^{\frac{2}{5}} \\ P_{\max -PF-i} = \left(\dfrac{5e \cdot m \cdot v^2}{4K_j}\right)^{\frac{2}{5}} \\ P_{\max -FN-N-i} = K_j^{\frac{2}{5}} \cdot \left\{\dfrac{m \cdot v^2}{2\left[\dfrac{2}{5e} \cdot + \dfrac{K_j \cdot y_i \cdot x_i \cdot \left(L^2 - x_i^2 - y_i^2\right)}{12E_2I_2L}\delta^{\frac{1}{2}}_{\max -FN(N-1)-i}\right]}\right\}^{\frac{2}{5}} \end{cases} \tag{36}$$

TABLE 1. Elastic parameters of the coal gangue and the metal plate.

Material	ρ (kg/m^3)	E (Pa)	μ
Coal	1380	5.12×10^9	0.3
Gangue	2400	9.966×10^9	0.28
Metal plate	7830	2.07×10^{11}	0.3

D. SYSTEM CONTACT FORCE UNDER MULTI-PARTICLES ELASTIC IMPACT

The basic elastic properties of coal gangue and the metal plate in this paper are shown in Table 1. Taking 10 particles impacting the metal plate simultaneously as the example. Sphere radius R is 0.025 m and RR is 0.1 m. The contact forces when the coal gangue particles with the volume ratio of 0%, 10%, 20%…, 90%, 100% elastic impacting the metal plate were calculated. The mixing order of 10 coal gangue particles is shown in Figure 8, and all of impact velocity are 3 m/s.

When coal gangue particles impact on the different positions of the metal plate, the relationship between the maximum contact force of the single coal gangue particle with the metal plate and the impact position is shown in Figure 9.

It is shown that the maximum contact force when coal gangue particle impact the metal plate in complete Hertz contact state and complete Flores contact state is unchanged with the change of impact position, while the maximum contact force fluctuates in the Hertz contact macroscopic deflection deformation state and the Flores contact macroscopic deflection deformation state. When the impact position is near the midpoint of the metal plate (in the direction of length), the maximum contact force decreases gradually. The maximum contact force in the midpoint of the length direction of the metal plate is the smallest, and the maximum contact force increases gradually when the impact position is close to both ends. Because of the existence of damping force and its energy dissipation, when impacting the same position of the metal plate, the maximum contact force produced by the impact of a single coal or gangue particle in the complete Flores contact state is less than that in the complete Hertz contact state, and the contact force in the Flores contact macroscopic deflection deformation state is less than that in the Hertz contact macroscopic deflection deformation state. Because of the deflection energy absorption of the metal plate, the contact forces of Hertz contact macroscopic deflection deformation state and Flores contact macroscopic deflection deformation state are much less than that of the complete Hertz contact state and complete Flores contact state when the same particle impacting the same position of the metal plate. Meanwhile, it can be seen from the figure that the contact force produced by the impact of gangue particle in four states is greater than that produced by the impact of coal particles when impact on the same position of the metal plate. According to the coal gangue mixing order in Figure 8 and Eqs. (35-36), the total contact force of the system under the undisturbed state is shown in Figure 10 when 10 coal gangue particles elastic impact on the metal plate simultaneously.

Figure 10 shows that the total contact force of the four contact systems increases with the increase of the gangue mixing ratio. Because the contact forces in the complete Hertz contact state and the complete Flores contact state are the same when the same single coal or gangue particle impacting the different position of the metal plate, the total contact forces of the complete Hertz contact and the complete Flores contact both increase linearly with the equal proportion increasing of the gangue mixing ratio. Hertz contact macroscopic deflection deformation state and Flores contact macroscopic deflection deformation state produce different contact force when the same single coal or gangue particle impact impacting the different position of the metal plate. Therefore, with the equal proportional increase of the gangue mixing ratio, the total contact force in the Hertz contact macroscopic deflection deformation state and Flores contact macroscopic deflection deformation state shows the fluctuating increase phenomenon.

III. SYSTEM RESPONSE WHEN MULTIPLE COAL GANGUE PARTICLES WITH BRITTLENESS IMPACTING THE FIXED METAL PLATE

Inevitably, as two kinds of rock, coal gangue have its own brittleness, it will damage or even break when it bears the impact force. The metal material has both elastic and plastic properties. Only calculating the elastic contact response when coal gangue impacting the metal plate, ignoring the energy loss and response changes caused by the damage, breakage or irreversible plastic deformation, will lead to the deviation in the study of the contact response when multiple particle impacting the fixed metal plate. Moreover, due to the random rebound of coal gangue after the collision and interference and influence between multi-particle collisions after the first impact, it is difficult to predict the re-collision between particles and metal plates by the simple elastic contact theory. Therefore, this section will take into account the brittleness of coal gangue, the elastoplasticity of the metal plate and the multi-point impact between multi-particles and the metal plate, and further study the vertical impact response of multiple coal gangue particles and the fixed metal plate by simulation.

A. SIMULATION OF MULTIPLE COAL GANGUE PARTICLES IMPACTING THE METAL PLATE

Establish the 3D model of multiple coal gangue particles impacting the metal plate in Solidworks. Among them, the metal plate is fixed by four screws and eight nuts on the upper (four) and lower (four) bottom surfaces. The specific size is shown in Figure 11. To ensure that the time synchronization and the first impact speed consistent, the shape effect of particles is consistent when modeling, that is, the shape and size of particles are exactly the same. In order to ensure that the initial contact state and the contact evolution mechanism of particles are the same, particles select the sphere. In the process of modeling, the total number of multiple coal gangue particles is the same, all of them are 10, and the radius

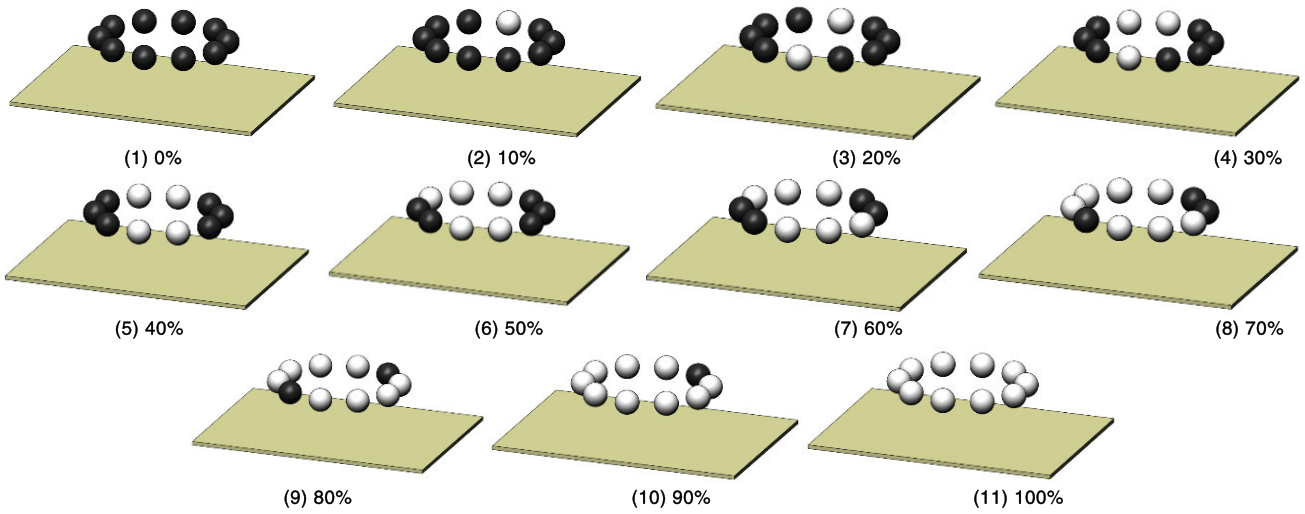

FIGURE 8. Mixing ratio of coal gangue and its location arrangement.

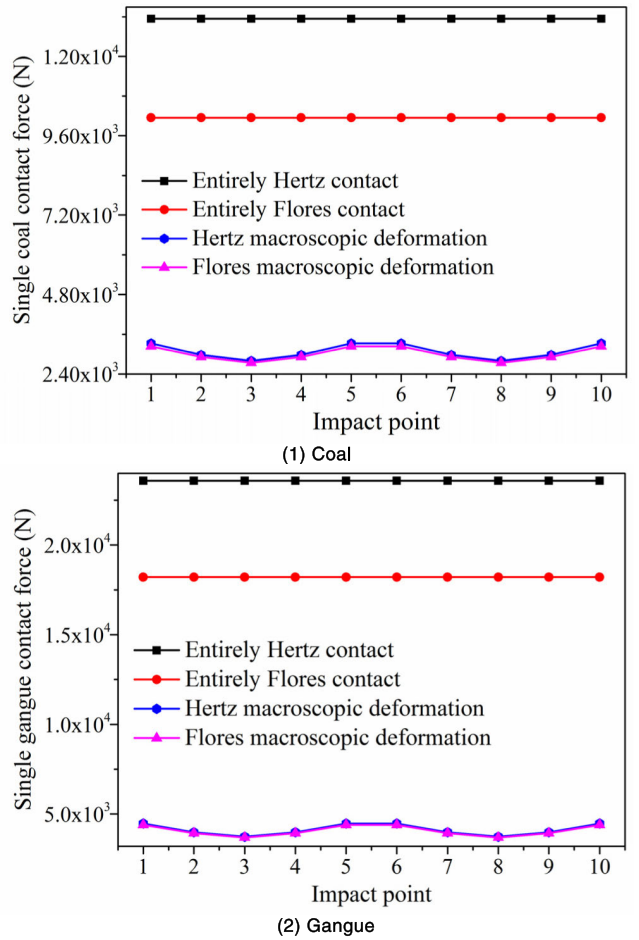

FIGURE 9. Maximum impact contact force when coal gangue particle impacting the different position.

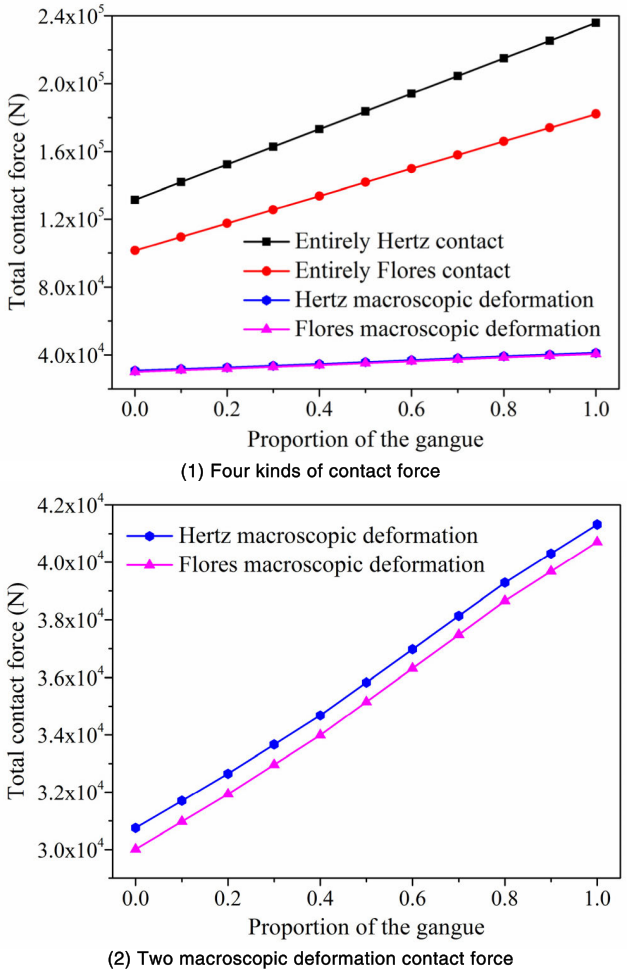

FIGURE 10. The system maximum total contact force when coal gangue mixed impacting the metal plate.

is 0.025 m. The lowest point of each particle sphere keeps a minimum distance from the upper surface of the metal plate, and the relative distance between the particles and the center of the metal plate is the same. The exact location is also shown in Figure 11. Then the model is imported into the simulation software Lsdyna. By changing the material properties of each sphere to change its coal gangue mixing ratio (in this paper refers to the volume ratio of coal gangue). The gangue mixing ratio is 0, 10%, . . . , 90%, 100%. Among them, J-H damage

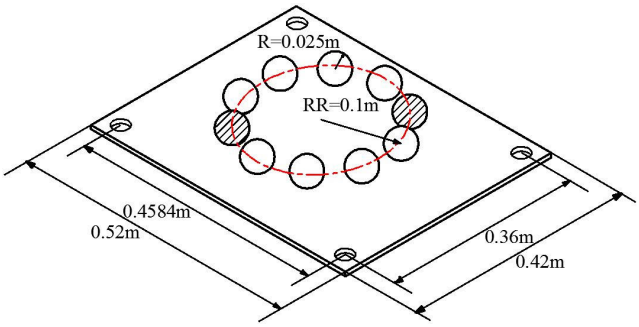

FIGURE 11. Diagram of the impact position.

FIGURE 12. Finite element model.

model is used for coal gangue, piecewise plastic model for the metal plate and elastic material for other materials.

The whole model is divided into hexahedral meshes, of which 10 particles have the same size and number of meshes, all of which are 10976 meshes. The metal plate is meshed after divided, and the mesh in the central area of the metal plate is encrypted. The total number of metal plate meshes is 97200. The gravity acceleration is defined as -9.8m/s^2 and the impact velocity is 3m/s. The contact mode between coal gangue and the metal plate is defined as surface-to-surface free contact, while the contact mode of other structural parts is TDNS. Model constraints are imposed on the bottom of four screw rods in the form of full constraints. The finite element model is shown in Figure 12.

B. ANALYSIS OF THE SIMULATION RESULTS

1) EFFECT OF GANGUE MIXING RATIO ON THE PARTICLES CONTACT RESPONSE

The vertical collision between coal gangue and the metal plate will be accompanied by the rebound of coal gangue and its re-collision with the metal plate. Taking the impact of 5 coal and 5 gangue on the metal plate as an example, the crushing state of spherical particles at different stages of the collision process with metal plate is obtained, as shown in Figure 13.

According to the figure, after the first collision, the broken area of single coal particle is much larger than that of gangue. Since the first collision, with the increase of the number of collisions, the degree of gangue breakage no longer changes, but the degree of coal breakage gradually increases.

For comparative analysis, according to the way shown in Figure 14, breakage areas of coal gangue particles after the first collision is extracted, and the breakage areas after the first collision of coal gangue with different mixing ratios are shown in Figure 15. It can be seen that the breakage area acreage of single coal or gangue particle does not change with the change of gangue mixing ratio. However, after the first collision, with the decrease of the gangue mixing ratio, the total breakage area acreage of 10 coal gangue particles increases gradually, and the breakage degree increases.

2) EFFECT OF GANGUE MIXING RATIO ON THE CONTACT RESPONSE OF THE METAL PLATE

In the process of collision, the contact response-time curves such as the displacement, velocity, acceleration and energy of the center of mass of the metal plate are shown in Figure 16 (a)-(f), respectively, and the change of the contact force between coal gangue and the metal plate is shown in Figures 17-18.

As shown in Figure 16, with the increase of the gangue mixing ratio, the vibration amplitude of the displacement, velocity and acceleration of the center of mass of the metal plate increases gradually, and the kinetic energy, internal energy and total energy of the metal plate increase, which shows that the increase of the gangue mixing ratio increases the energy obtained by the metal plate under impact. According to the contact force-time curve between single coal or gangue (all at 3# position) and the metal plate in Figure 17, the contact force between single particle and the metal plate after gangue impacting metal plate is larger than that of coal when impact at the same position, which is consistent with the conclusion calculated by the elastic impact theory in Figure 7. However, the time lags behind that of coal after gangue re-collision with the metal plate. From Figure 18, it can be seen that the total contact force between coal gangue particles and the metal plate increases gradually with the increase of gangue mixing ratio. At the same time, the collision between each particle and the metal plate is not synchronized since the second collision. The maximum values of each contact response in Figure 16 and Figure 18 are extracted, and the maximum contact response-gangue mixing ratio curve is obtained, as shown in Figure 19. It can be learn that in the process of collision and crushing between gangue and metal plate, with the increase of gangue mixing ratio, the two-way maximum displacement, velocity and acceleration of the metal plate increase, and the total maximum contact force and each part of energy also increase.

Comparing Figure 10 and Figure 19 (4), due to the particle breakage and its energy loss are not taken into account in the theoretical modeling process, it can be seen that the maximum total contact force obtained by the four contact theories of the complete Hertz contact state, the complete Flores contact state, the Hertz contact macroscopic deflection deformation state and the Flores contact macroscopic deflection deformation state is much larger than that of the simulation. Flores contact macroscopic deflection deformation state takes into

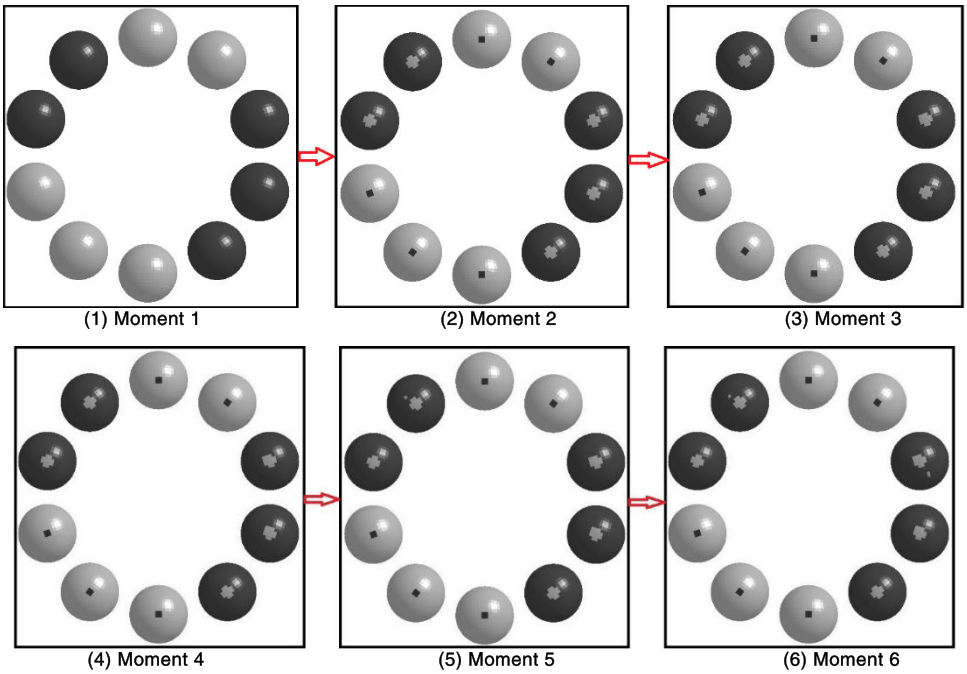

FIGURE 13. Breakage state of coal gangue at different impact stages (5 coal 5 gangue).

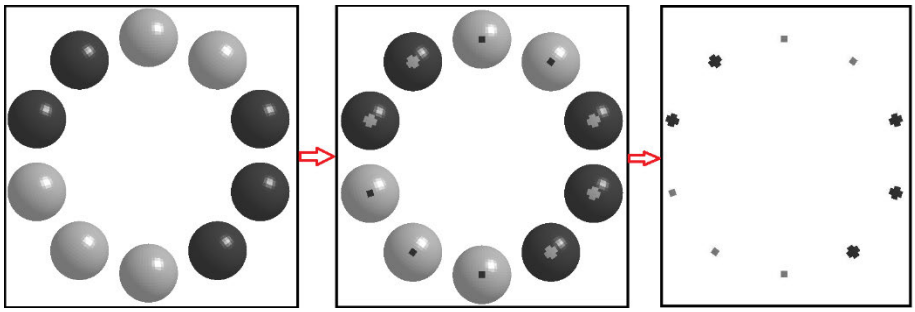

FIGURE 14. Schematic diagram of the extraction of coal gangue particle breakage area (5 Coal 5 Gangue).

account the influence of the damp dissipation force and the energy absorption of metal plate, so the difference of the maximum contact force obtained by the theory of Flores contact macroscopic deflection deformation state and the maximum contact force obtained by the simulation is the smallest. Therefore, the theory of the Flores contact macroscopic deflection deformation state is more suitable for predicting the contact force when multi-particles elastic impacting the metal plate simultaneously.

According to the location of the stress extraction point in the metal plate shown in Figure 20, stress nephograms of the contact area of the metal plate contacting with the 10 particles with the different gangue mixing ratio are extracted respectively, as shown in Figure 21 (1) - (11).

According to the figures, when the particle is mainly coal (the gangue mixing ratio is less than 20%), the color of the stress nephogram is relatively simple, mainly composed of blue, cyan and green. When the gangue mixing ratio is more than 20%, with the increase of the gangue mixing ratio, the acreage of yellow and red areas in the stress nephogram increases gradually, that is, overall stress value increases gradually. The red region which completely crosses the whole stress nephogram section in the stress nephogram is defined as the high stress region. When the gangue mixing ratio exceeds 70%, the high stress region appears in the stress nephogram and its area increases continuously with the increase of the gangue mixing ratio. The change of the gangue mixing ratio significantly affects the color composition of the stress nephogram.

IV. TIME-FREQUENCY DOMAIN CHARACTERISTICS ANALYSIS OF THE METAL PLATE VIBRATION SIGNALS

In order to further understand the influence of gangue mixing ratio on the contact response, the vibration acceleration signal of the metal plate is taken as the object to the time-frequency domain analysis. The time step in the simulation is set to 0.00015s, therefore, the sampling frequency used in the signal analysis process is 6667 Hz. After EMD

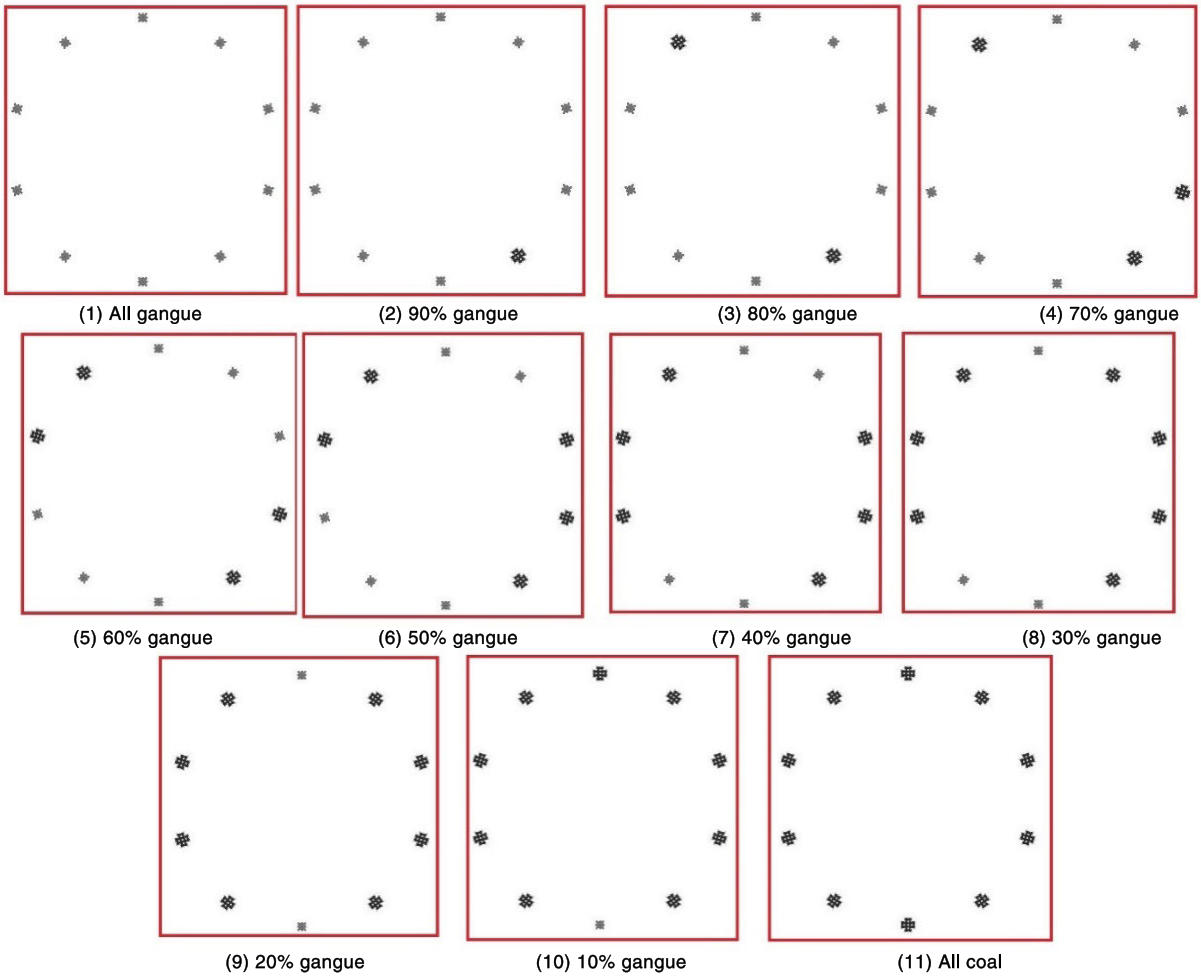

FIGURE 15. Breakage state after the particles with different gangue mixing ratio first impacting the metal plate.

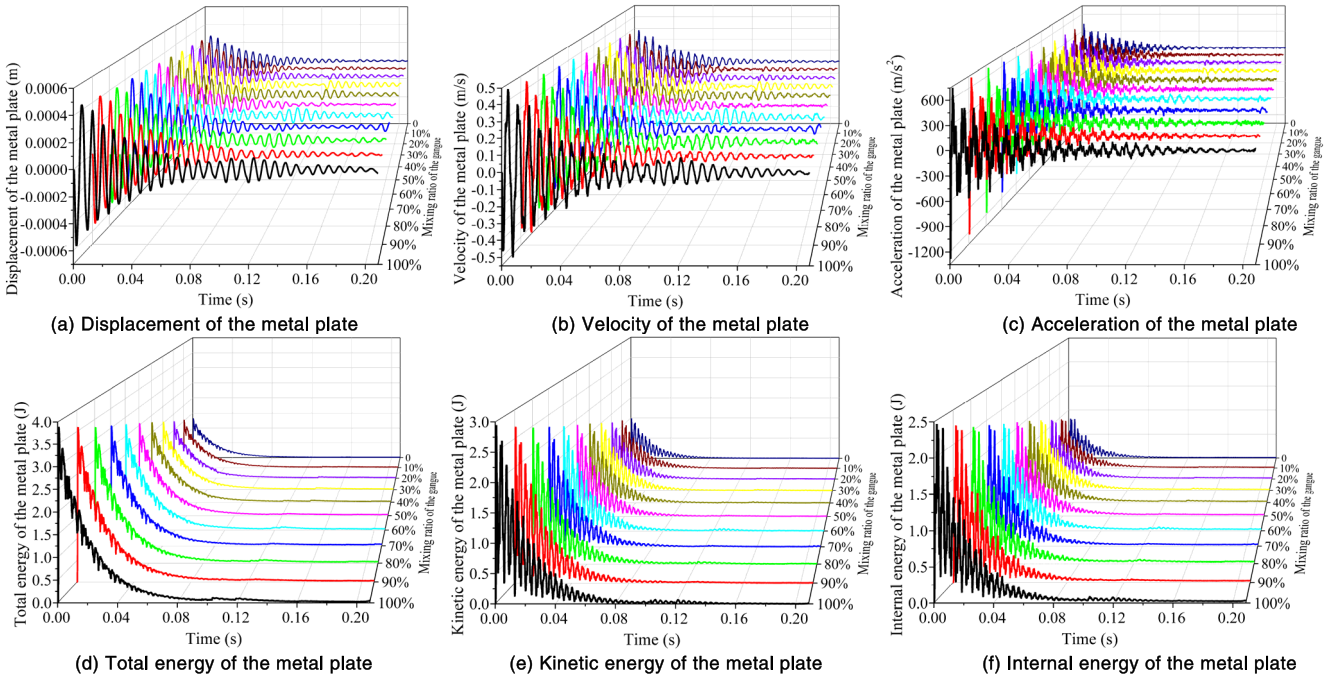

FIGURE 16. Vibration response characteristics of the metal plate.

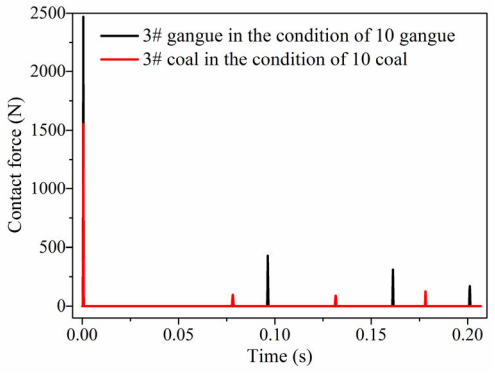

FIGURE 17. Single Contact force.

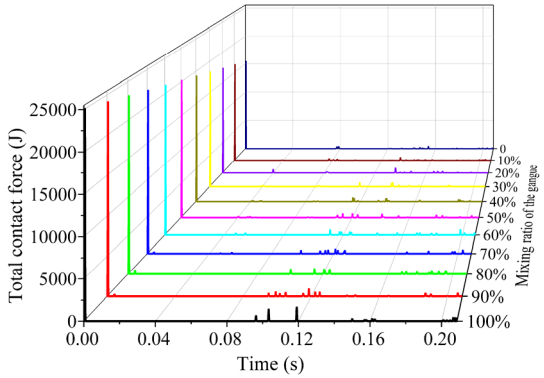

FIGURE 18. Total contact force.

decomposition [8], [49]–[62], IMF components of the acceleration is obtained, as shown in Figure 22.

According to the figures, the number of IMF components decomposed from the acceleration signal of the metal plate is different when coal gangue mixing ratio is different. The maximum values of IMF 1 in both positive and negative directions increase with the increase of gangue mixing ratio, however, with the increase of gangue mixing ratio, other IMF components do not show a regular pattern. According to Figure 22 and the calculation methods of the traditional time-domain parameters, energy eigenvalues of IMF components and energy values of the Hilbert marginal spectrum of signals in reference [8], the energy eigenvalues of the IMF component, the square root amplitude, . . . , and the energy value of the Hilbert marginal spectrum and other time-frequency parameters of the metal plate acceleration signal under multi-particles impact is obtained respectively, their changing curves with the change of the gangue mixing ratio are shown in Figure 23.

From the figures, with the increase of gangue mixing ratio, the energy characteristic value of the IMF components, mean value, waveform index and kurtosis index of the vibration acceleration signal are disorderly changing. The square root amplitude, absolute mean value, variance, peak-to-peak value, root mean square value and the marginal spectral energy value show the increasing trend as a whole, while the skewness and the margin index show the downward trend as a whole.

V. RECOGNITION OF COAL GANGUE MIXING RATIO

A. RECOGNITION OF COAL GANGUE MIXING RATIO BASED ON TIME-FREQUENCY PARAMETERS FUSION OF VIBRATION ACCELERATION

The square root amplitude, absolute mean value, variance, peak-to-peak value, root mean square value, marginal spectral energy value, skewness and margin index of the metal plate vibration acceleration show the monotonic trend as a whole, therefore, taking these eight kinds of data as the time-frequency base parameters of the acceleration signal, the coal gangue mixing ratio recognition based on the time-frequency parameter samples of vibration acceleration is carried out.

1) DATA STANDARDIZATION TREATMENT

The data indexes represented by the time-frequency domain parameters are different, the order of magnitude and unit of each parameter is different. For data fusion, the parameters need to be normalized. On account of the data type in the paper, the signal is normalized by the minimum-maximum standardization method. Treatment standard is:

$$X^* = \frac{x_s - x_{\min}}{x_{\max} - x_{\min}} \tag{38}$$

Among them, $x_{\max}$ is the maximum value of sample data, $x_{\min}$ is the minimum value of sample data, x_s is the sample data, and X^* is the value standardized by the sample data x. The trend of data obtained by Equation (38) is consistent with that before the standardization treatment. However, there are two different trends in the data (approximate increasing and approximate decreasing). To facilitate data fusion, the standardized treatment standard in this paper is proposed as follows by extending the Equation (38):

$$X^* = \begin{cases} \dfrac{x_s - x_{\min}}{x_{\max} - x_{\min}}, & \text{Increase/Approximate increase} \\ \dfrac{x_s - x_{\max}}{x_{\min} - x_{\max}}, & \text{Decrease/Approximate decrease} \end{cases} \tag{39}$$

According to this, the values of the square root amplitude, absolute mean value, variance, peak-to-peak value, root mean square value, marginal spectrum energy value, skewness and margin index after the minimum-maximum standardization processing are obtained as shown in Table 2.

2) RECOGNITION OF COAL GANGUE MIXING RATIO BASED ON ACCELERATION MULTI-TIME-FREQUENCY PARAMETERS FUSION

After the determination of the time-frequency base parameters and the standardized processing, the ranges of the different time-frequency domains parameters are unified to [0, 1]. Then, data fusion based on multi-time-frequency parameters of acceleration is proposed by linear superposition method. The fusion recognition parameter is defined as Q, the square

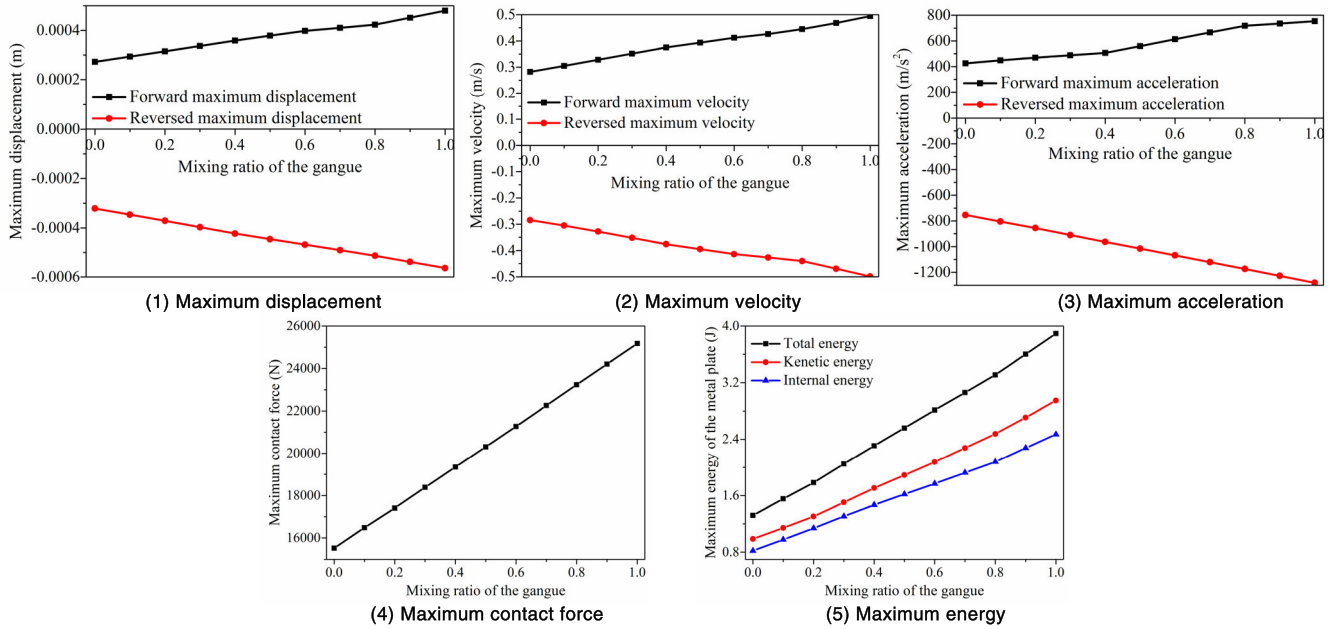

FIGURE 19. Maximum contact responses.

TABLE 2. Standardization processing on time-frequency base parameters of the acceleration signal.

Base parameters	0	10%	20%	30%	40%	50%	60%	70%	80%	90%	100%
Square root amplitude	0	0.0561	0.106	0.237	0.323	0.353	0.488	0.502	0.720	0.702	1
Absolute mean value	0	0.0784	0.144	0.303	0.396	0.429	0.564	0.577	0.774	0.758	1
Variance	0	0.0712	0.136	0.240	0.334	0.413	0.516	0.606	0.733	0.838	1
Peak-to-peak value	0	0.0860	0.170	0.255	0.339	0.462	0.586	0.709	0.832	0.916	1
Root mean square value	0	0.0950	0.176	0.298	0.401	0.482	0.583	0.667	0.780	0.870	1
Marginal spectrum energy value	0	0.0191	0.188	0.255	0.2579	0.368	0.428	0.562	0.730	0.747	1
Skewness	0	0.0547	0.112	0.187	0.271	0.365	0.468	0.583	0.710	0.848	1
Margin index	0	0.158	0.263	0.572	0.696	0.619	0.719	0.631	0.811	0.762	1

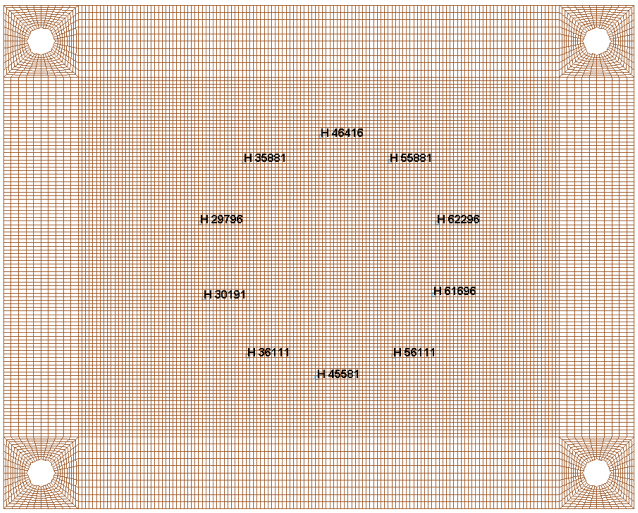

FIGURE 20. Stress extraction point in the metal plate.

root amplitude, absolute mean value, variance, peak-to-peak value, root mean square value, marginal spectral energy value, skewness and margin index of the metal plate vibration acceleration is $x_1, x_2, \ldots, x_7, x_8$ respectively, and their linear contribution coefficients is $\alpha_1, \alpha_2, \ldots, \alpha_7, \alpha_8$ ($\sum \alpha_i = 1$, $i = 1, 2, \cdots, 8$) respectively (To characterize the contribution of each time-frequency parameter to the fusion recognition parameter Q), then:

$$Q = \alpha_1 x_1 + \alpha_2 x_2 + \alpha_3 x_3 + \alpha_4 x_4 + \alpha_5 x_5 + \alpha_6 x_6 + \alpha_7 x_7 + \alpha_8 x_8 \quad (40)$$

In this paper, we define that each base parameter has the same effect on the fusion recognition parameter Q, i.e. $\alpha_i = 0.125$. Under the condition of different gangue mixing ratio, the fusion recognition parameter curve based on the acceleration multi-time-frequency parameters is shown in Figure 24.

From Figure 24, with the increase of the gangue mixing ratio, the fusion recognition parameter Q based on the acceleration multi-time-frequency parameters increases gradually, according to the data of the fusion recognition parameter Q at different mixing ratios, the relation equation between Q and the gangue mixing ratio β is $y = 0.00614 + 0.79954 \cdot \beta + 0.15488 \cdot \beta^2$. The coefficient of determination of the relation equation $R^2 = 0.99079$, which indicates that the fitting curve's reliability of the fusion recognition parameters based on acceleration multi-time-frequency parameters is

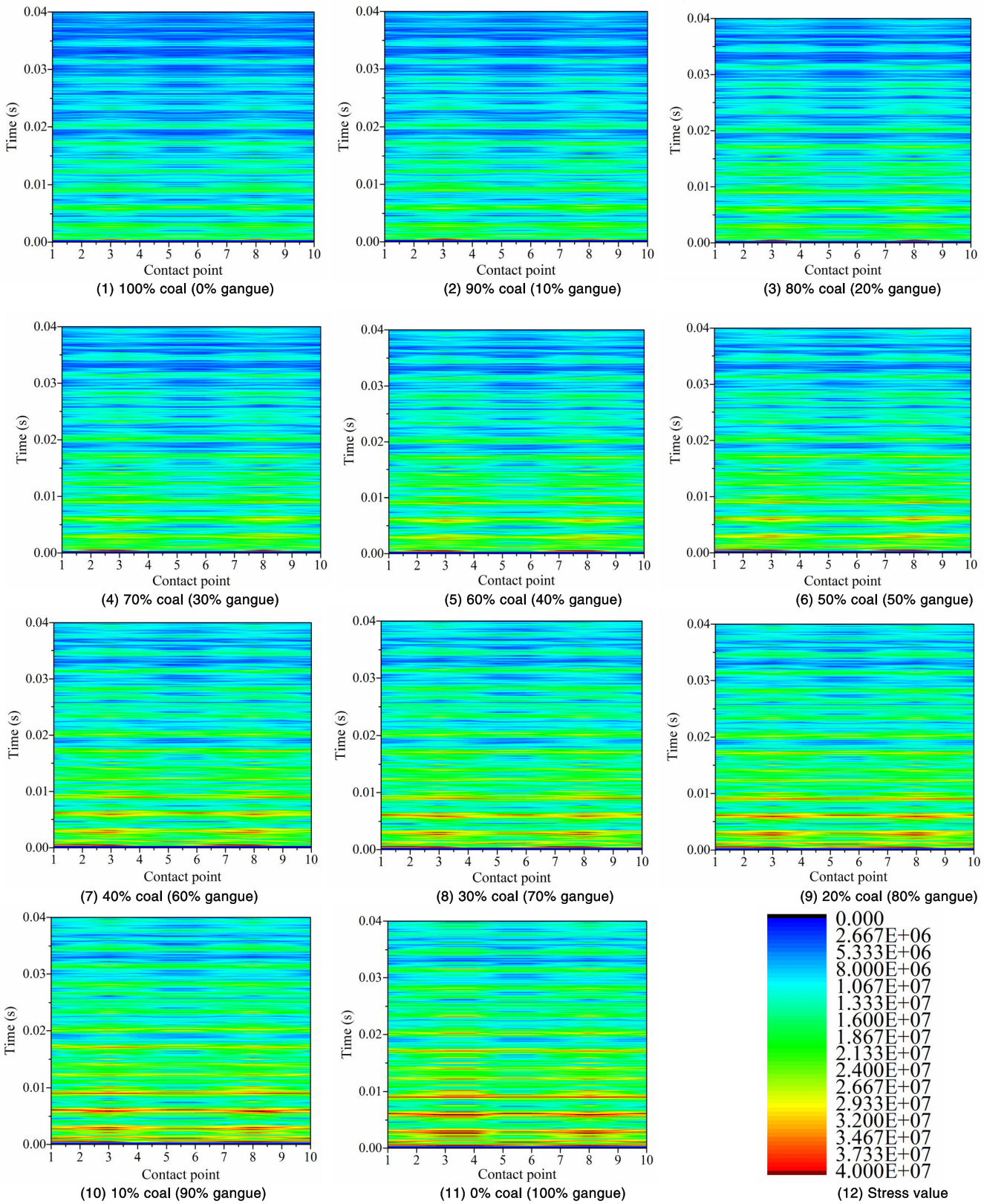

FIGURE 21. Stresses at contact points of the metal plate.

very high, and fusion recognition parameter Q obtained from the relation equation is close to the measured values.

However, from the figure, the curve of the relation equation still deviates from the measured value of Q. As shown

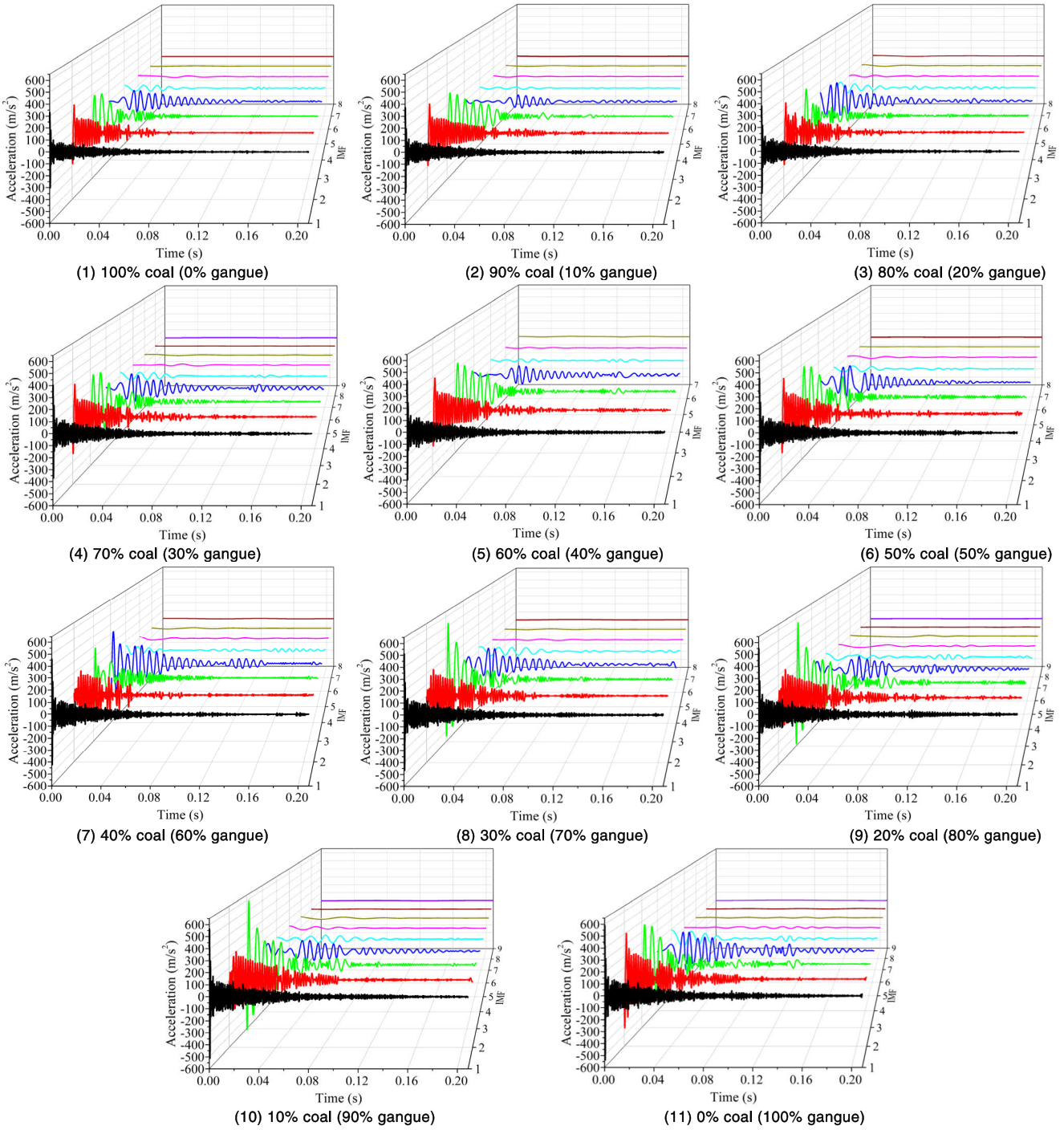

FIGURE 22. IMF components of the acceleration of metal the plate.

in Table 3, the degree of deviation varies from 0.00614 to 0.0459728, and there are positive and negative deviations. Fusion recognition parameter Q based on acceleration multi-frequency parameters is only a point parameter value, and it is calculated only according to the 11 groups measured Q values with different mixing ratio. When calculating the gangue mixing ratio based on the relationship equation and the measured value of the fusion recognition parameter Q obtained from other simulation, especially when the actual mixing ratio is close to $[0, 10\%, \ldots, 90\%, 100\%]$, there will be a large deviation (For example, the calculated value of Q according to the relational equation is 0.0876428, but the measured value of Q when the gangue mixing ratio is 10% is only 0.077357, which the gangue mixing ratio only corresponds to 8.7586% through the relation equation, then the difference of the calculated mixing ratio is 1.2414% from

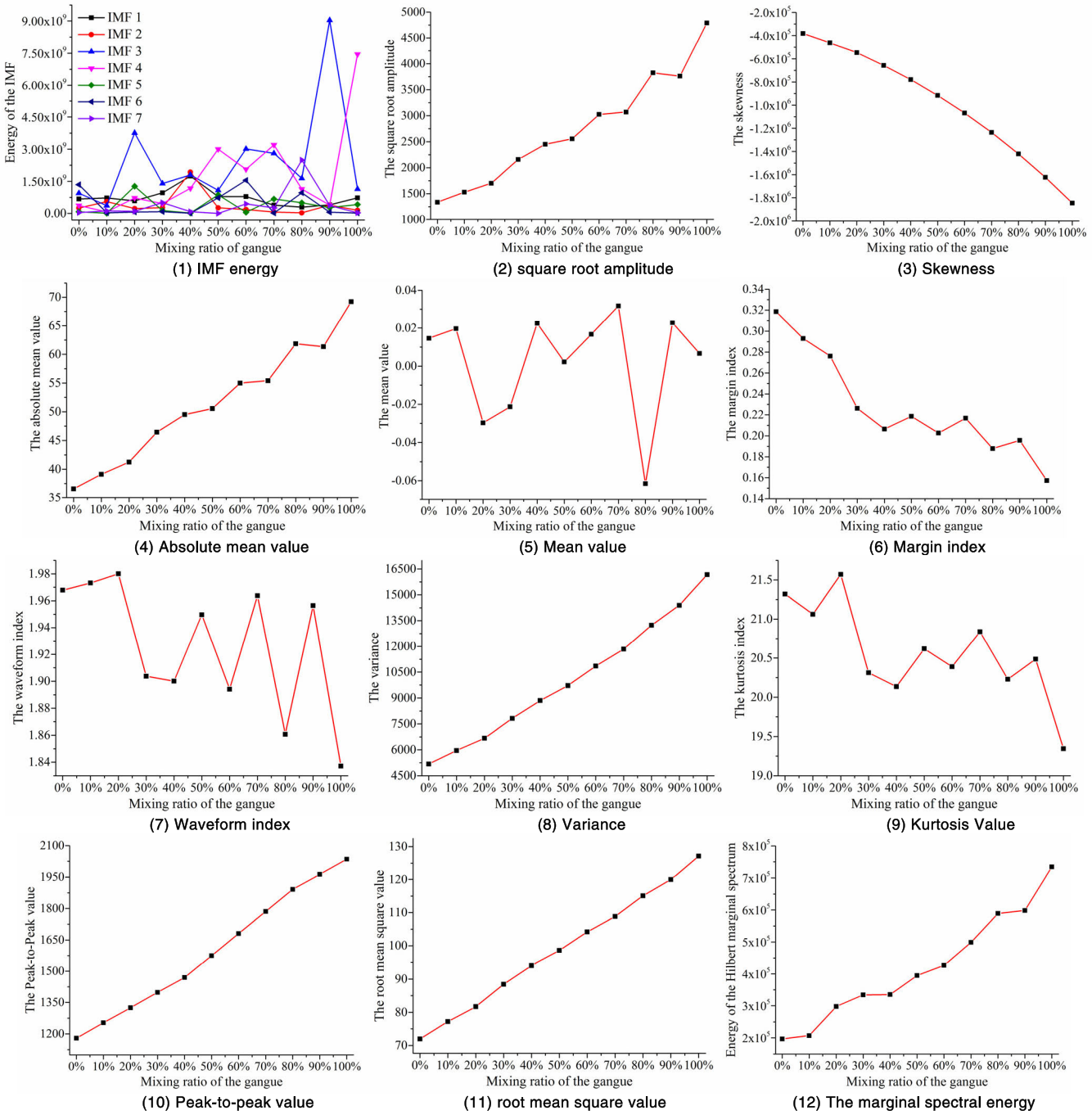

FIGURE 23. Time-frequency parameters of the metal plate vibration acceleration.

the actual one). Therefore, fusion recognition parameter Q based on acceleration multi-time-frequency parameters and its relationship equation is just more suitable for the prediction of coal gangue mixing ratio.

B. RECOGNITION OF COAL GANGUE MIXING RATIO BASED ON MULTI-RESPONSE INFORMATION FUSION

Fusion recognition parameter Q based on the acceleration multi-time-frequency parameters can roughly estimate the mixing gangue ratio, which is suitable for the places where the accuracy of the gangue mixing ratio calculation is not high. In order to improve the recognition accuracy of coal gangue mixing ratio, a method based on Kalman filter and multi-information fusion is proposed to identify coal gangue mixing ratio.

1) KALMAN FILTER PROCESSING TO THE METAL PLATE SIGNALS

Kalman filter [63]–[67] is a widely used filtering method, it can obtain the system states or real signals by processing

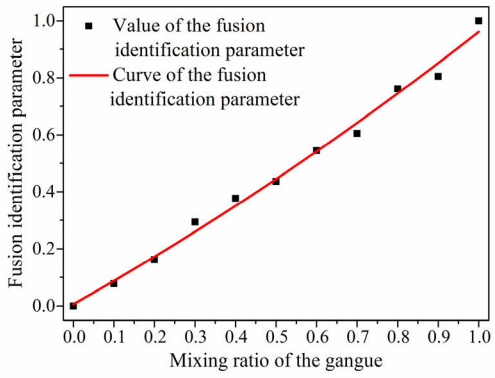

Mixing ratio of the gangue	Q	Mixing ratio of the gangue	Q
0	0	60%	0.5441
10%	0.077357	70%	0.604659
20%	0.161858	80%	0.761186
30%	0.293548	90%	0.805206
40%	0.37705	100%	1
50%	0.436385		

FIGURE 24. Acceleration-based fusion recognition parameter Q.

TABLE 3. The deviation degree of Q obtained by the relation equation.

Gangue mixing ratio	0	10%	20%	30%	40%	50%	60%	70%	80%	90%	100%
Measured value	0	0.0774	0.162	0.294	0.377	0.436	0.544	0.605	0.761	0.805	1
Calculated value	0.00614	0.0876	0.172	0.260	0.351	0.445	0.542	0.642	0.745	0.851	0.961
Difference value	0.00614	0.0103	0.0104	-0.0336	-0.0263	0.00825	-0.00248	0.0371	-0.0163	0.0460	-0.0394

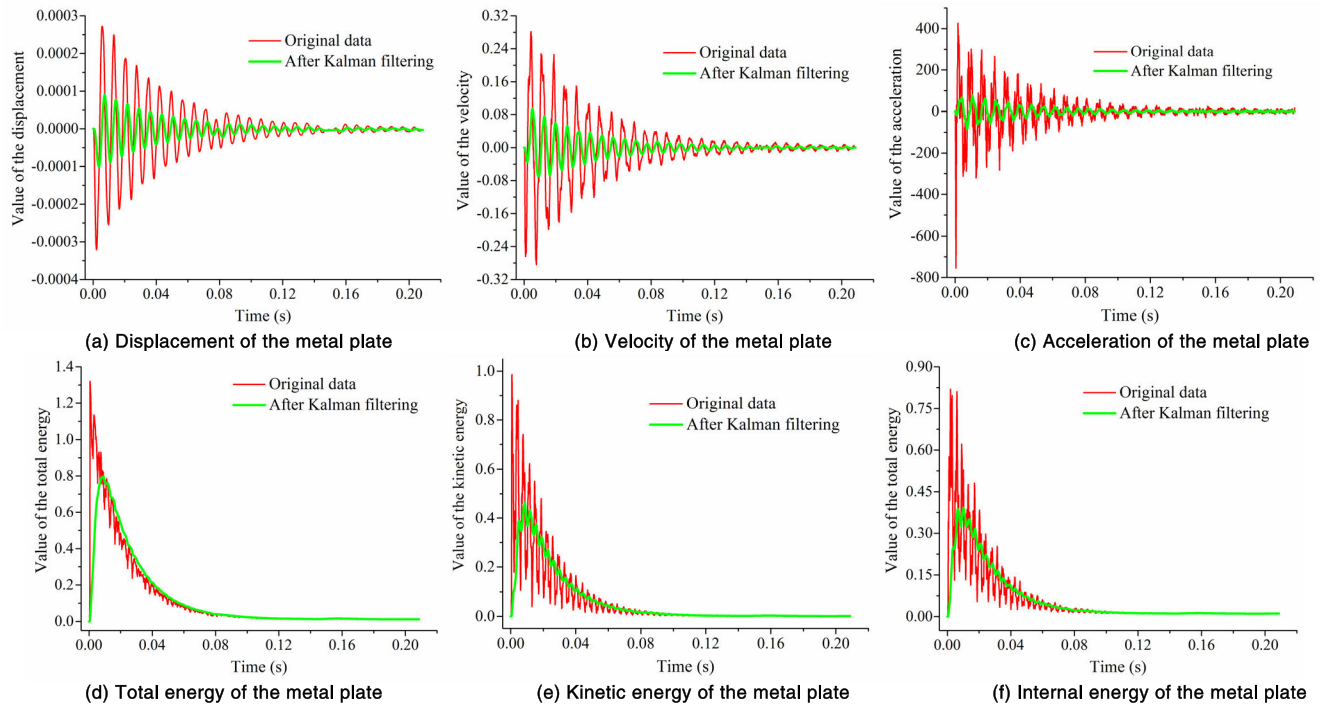

FIGURE 25. Kalman filter to the metal plate signals under 10 coal impact.

the input and observed signals which contains the noise. From Figures 16 (a) - (f), after the metal plate is impacted by coal gangue, the displacement, velocity, acceleration and each part of energy of the metal plate all present the fluctuating curves, which conceal some characteristics of the contact responses. Therefore, Kalman filter is adopted in this paper to process them respectively.

Taking the 10 coal particles (gangue mixing ratio is 0) impacting the metal plate as the example, the displacement, velocity, acceleration, total energy, kinetic energy and internal energy of the metal plate after the impact of coal are treated, the Kalman filter curves of the metal plate response signals when the 10 coal particles impact is obtained, as shown in Figure 25. From the figures, after Kalman filtering, the fluctuation frequency and vibration amplitude of each contact response decrease correspondingly, and the contact responses tend to stabilize.

According to the method shown in Figure 25, Kalman filtering was performed on the total energy of the metal plate after impact of coal gangue with different mixing ratios respectively, the total energy of the metal plate before and after filtering is obtained as shown in Figure 26. As can

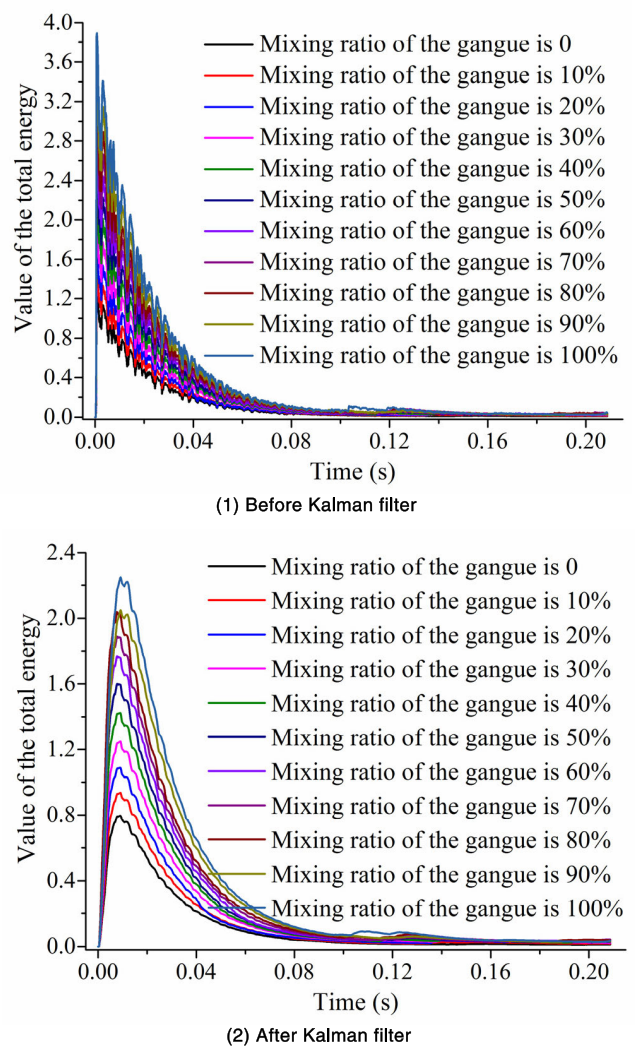

FIGURE 26. Total energy of the metal plate.

be seen from the figure, through Kalman filtering, the total energy curves of metal plates under the impact of coal gangue with different mixing ratios are more clearly stratified than that of before Kalman filtering, the degree of the differences is enlarged, and the overlap degree of the curves is reduced. However, in the filtering process, the peak of the total energy filtering curve appears to be partially crossed when the gangue mixing ratio is 90% and 100%.

After filtering the other five contact responses, the filter curves of the metal plate signals as shown in Figure 27 are obtained. According to the figures, after filtering, the stratified difference of the kinetic energy and internal energy curves of the metal plate under the impact of coal gangue particles with different gangue mixing ratios are more distinct, the maximum value increases with the increase of the gangue mixing ratio, but the degree of stratification is still small. The fluctuation amplitude and vibration tendency of the acceleration, velocity and displacement of the metal plate change to some extent, the amplitude of acceleration, velocity and displacement filtering curve of metal plate does not change monotonously with the change of gangue mixing ratio. The feasibility is low to realize the coal gangue mixing ratio recognition only relying on Kalman filter to filter a single signal, the single signal Kalman filtering method can be used as a tool to amplify the differences.

2) MULTI-RESPONSE SIGNALS FUSION OF THE METAL PLATE BASED ON KALMAN FILTER

In order to improve the recognition rate of gangue mixing ratio, in this paper, Kalman filter and multi-information fusion method are combined to carry out the gangue mixing ratio fusion recognition based on Kalman filter. For the fusion of signals, different types of signals need to be normalized processing firstly. The normalized processing criterion of the metal plate response is:

$$y_{ij}^{*} = \frac{y_{ij} - y_{ij\min}}{y_{ij\max} - y_{ij\min}} \tag{41}$$

Among them, y is the signal, i is the column label of the signal ($i = 1, 2 \cdots, 10, 11$, respectively corresponding to the gangue mixing ratio of 0, 10%, ..., 100%), j is the label of the j[th] sample point of each column of signals ($j = 1, 2 \cdots, 3999, 4000$), y_{ij} is the value of the j^{th} sample point of the i^{th} column y signal, $y_{ij\min}$ and $y_{ij\max}$ are the maximum and minimum values of all sample points of y signal (there are 11 types of gangue mixing ratio, 0,10%, ...,100% respectively, so each kind of signal has 11 columns, $y_{ij\min}$ and $y_{ij\max}$ are the maximum and minimum values in all 11 columns of y signal). Taking the total energy of the metal plate as the example, the normalized total energy parameters are shown in Figure 28.

The acceleration, velocity, displacement, internal energy, kinetic energy, total energy, absolute value of acceleration, absolute value of velocity and absolute value of displacement are normalized respectively. After the normalization process, the variation interval of all 9 groups of parameters is [0, 1]. Among the 9 sets of parameters, the changing form of the normalized internal energy, normalized kinetic energy and normalized total energy is similar, the changing form of the normalized acceleration, normalized velocity, and normalized displacement is similar. The changing form of the normalized absolute value of the acceleration, normalized absolute value of the velocity, and normalized absolute value of the displacement is similar. And the changing form of the normalized energy are close to the normalized absolute value of the other responses (acceleration, velocity, and displacement), Therefore, in this paper, Kalman filter-based data fusion is applied to these four combined signals, which are defined as the energy fusion, the other response fusion, the fusion of the absolute value of the other responses and the composite response fusion respectively.

Taking the response signals of the metal plate under the 10 coal particles impact as an example, the normalized energy signal fusion process, the normalized other responses (acceleration, velocity and displacement) fusion process, the fusion process of normalized absolute value of the other responses

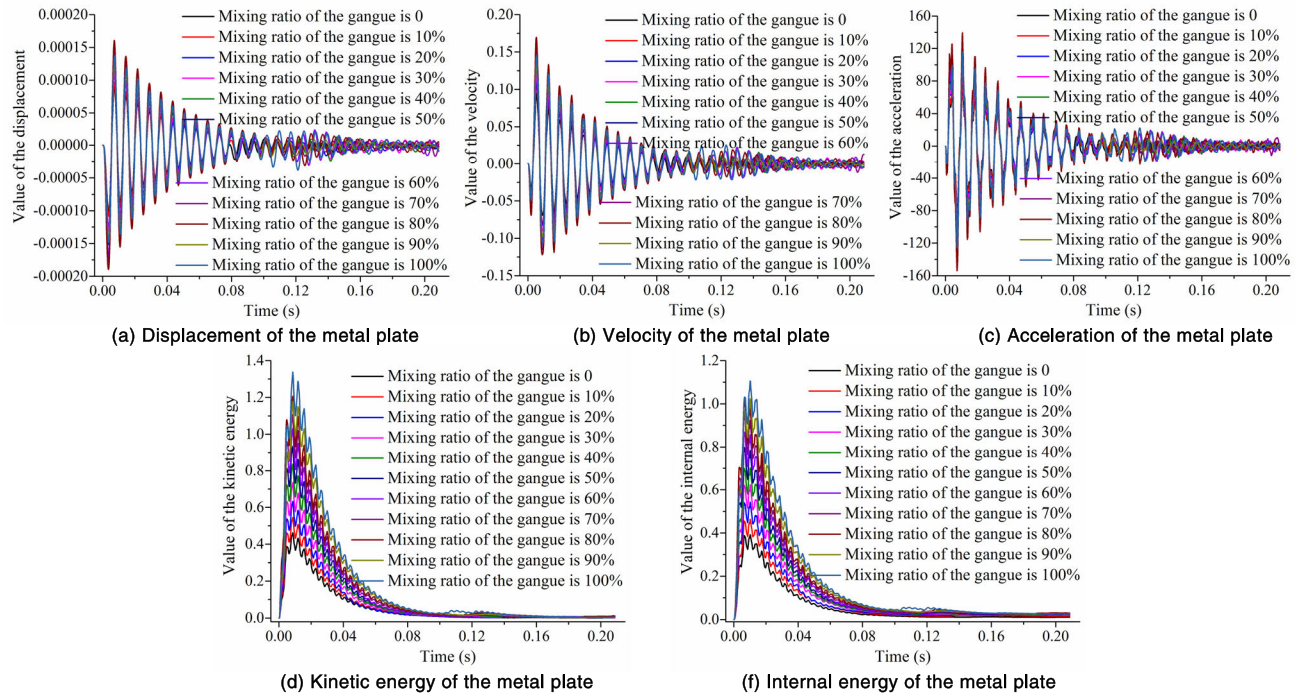

FIGURE 27. Signals of the metal plate after Kalman filtering.

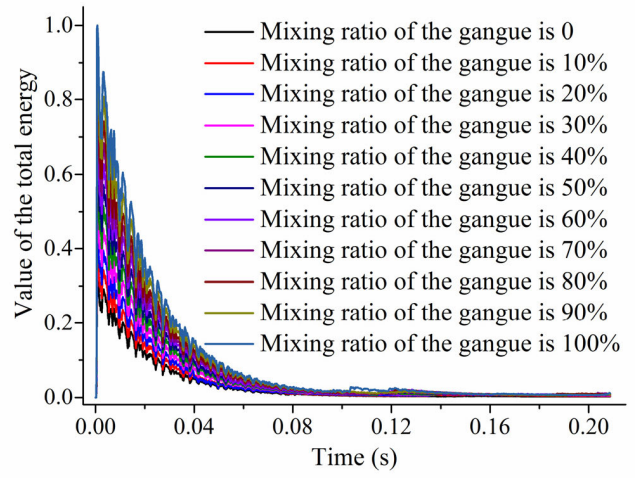

FIGURE 28. Normalization of the metal plate total energy.

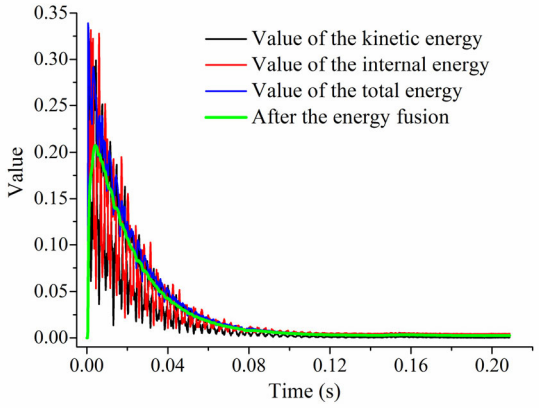

FIGURE 29. Energy fusion process.

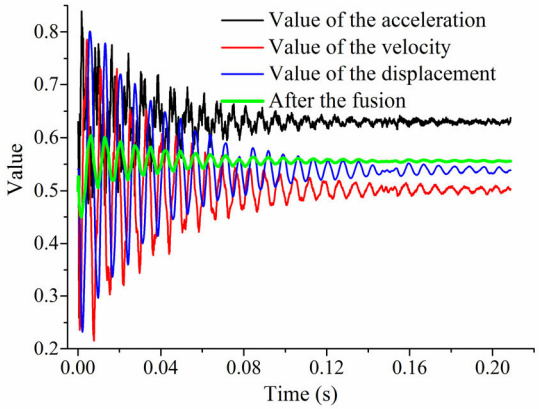

FIGURE 30. Other responses fusion process.

(acceleration, velocity and displacement), and the composite fusion process of the six sets of parameters (energy, acceleration, velocity and displacement) after normalized are obtained, as shown in Figures 29-32 respectively. It can be seen from the figure that the fluctuation amplitude of the signal is greatly reduced after the fusion, the fused signal is in the variation region of various signals and the signal is more stable.

The above four kinds of signals fusion based on Kalman filter were carried out on the metal plate signals with different gangue mixing ratio respectively, and the fusion curves shown in Figures 33-36 were obtained. Due to the existence of re-collision between particles and the metal plate, only the data changing trend within 0∼0.04s is considered. After four kinds of data fusion, the maximum values (or reverse

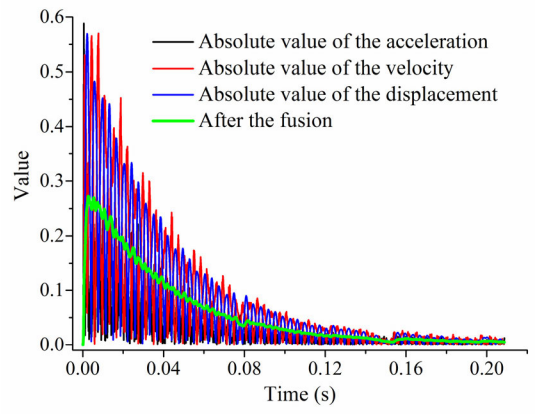

FIGURE 31. Absolute value fusion of other responses.

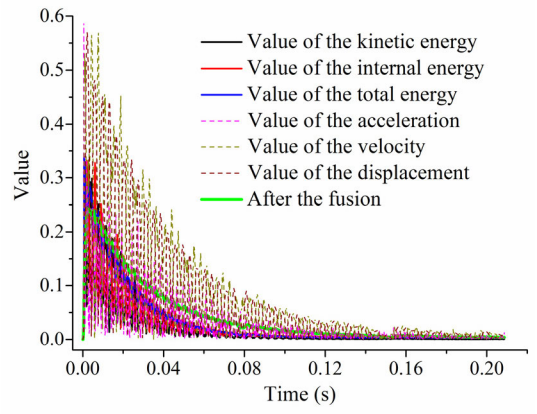

FIGURE 32. Composite fusion.

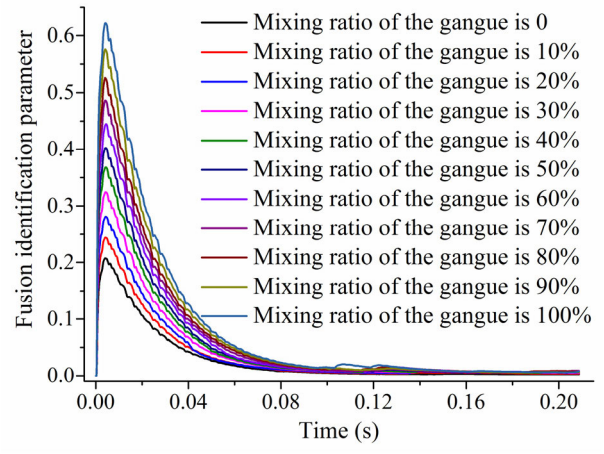

FIGURE 33. After energy fusion.

maximum values) of the four groups of composite fusion parameters gradually increased with the increase of gangue mixing ratio, the fusion parameter curve formed by the changing of the gangue mixing ratio in 0∼0.3s shows uncrossed stratification and very low overlap. Compared the four kinds of data fusion methods, the fusion parameter differences between the other response fusion and the fusion of the absolute value of the other responses is still small, some crossing and overlapping phenomena still exist after 0.3s in the fusion

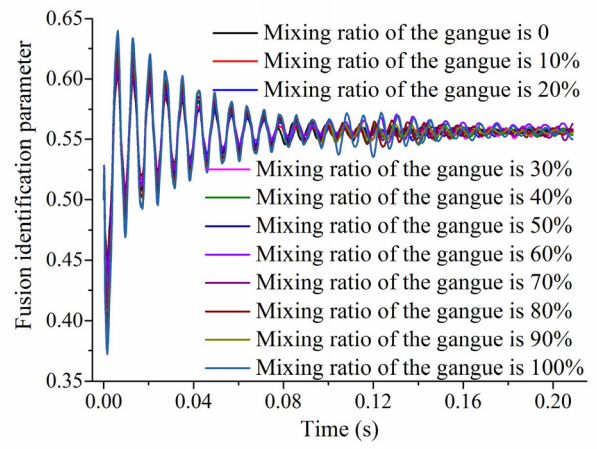

FIGURE 34. After other responses fusion.

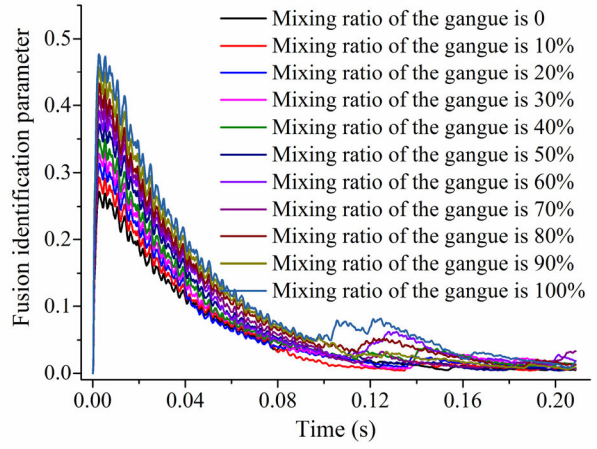

FIGURE 35. After absolute value fusion of other responses.

of the absolute value of the other responses. After energy fusion and composite fusion, the fusion parameter curves of different gangue mixing ratio are stratified more obvious. Compared with the composite fusion mode, the energy fusion mode presents a single peak trend, the fusion parameter curve is less volatile and more stable, so the stratification phenomenon is more significant and the differences are higher. Therefore, energy fusion is adopted to the process of the signals.

3) COAL GANGUE MIXING RATIO RECOGNITION STRATEGY BASED ON KALMAN FILTER AND ENERGY FUSION

Defined the parameter after energy fusion is energy fusion parameter QQ. After processing the signal by Kalman filter and energy fusion, QQ needs to be further processed and analyzed. On this basis, this paper proposed a recognition strategy of coal gangue mixing ratio based on Kalman filter and energy fusion, so as to accurately realize the coal gangue mixing ratio recognition. After in-depth analysis of Figure 33, this paper proposes the following processing methods and recognition strategies:

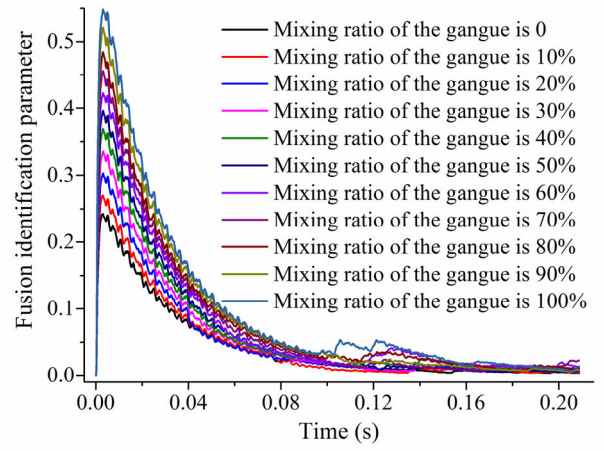

FIGURE 36. After the composite fusion.

(1) Within 0∼0.04s, each energy fusion curve includes 267 sample points (The time interval is 1.5×10^{-4}s and it should be 266.7 points within 0.04s, the simulation software error results in 267 sample points to be covered), corresponding to 267 different moments respectively. In this paper, there are 11 energy fusion curves when the gangue mixing ratio gradually changes from 0 to 100%. Therefore, 267 relational broken lines between energy fusion parameter QQ and gangue mixing ratio β can be obtained by the discretizing, every relational broken line has 11 discrete points.

(2) The polynomial curve fitting was carried out for 267 relational broken lines between QQ and β respectively, and 267 functional polynomials between QQ and β at different moments were obtained. They are respectively defined as the No. 1 energy fusion function QQ_1, No. 2 energy fusion function $QQ_2, \ldots,$ No. 267 energy fusion function QQ_{267}, and correspond to different moments respectively. The function form is $QQ = a \cdot \beta^m + b \cdot \beta^{m-1} + \cdots + aa \cdot \beta + bb$ (Where, $m \geq 1$, $a, b, \ldots, aa$ are the coefficients of the functional polynomial respectively, and bb is the constant term of the polynomial), the coefficient of determination R^2 of each fitting curve requires more than 99% (Or more higher).

(3) When estimate the coal gangue mixing ratio according to the energy fusion curve of the metal plate, the sample point values corresponding to the first 267 moments of the target energy fusion curve are discretized to 267 energy fusion parameter values corresponding to different moments, it was respectively defined as Point 1, Point $2, \ldots,$ Point 267 according to the increase of time, and the corresponding energy fusion parameter is QQ_{Point1}, $QQ_{Point2}, \ldots,$ $\mathrm{QQ_{Point267}}$. By inversely substituting QQ_{Point1} into the No. 1 energy fusion function QQ_1, the calculated value $\beta_1$of gangue mixing ratio can be obtained by the inverse solution. Then substitute β_1 into function QQ_2, $QQ_3 \ldots, QQ_{267}$, get its calculated value $QQ_{2-\beta_1}$, $QQ_{3-\beta_1} \ldots, QQ_{267-\beta_1}$, and the absolute differences between the calculated value of the energy fusion function and the value of the energy fusion parameter are obtained respectively as $\left|QQ_{2-\beta_1} - QQ_{Point2}\right|$, $\left|QQ_{3-\beta_1} - QQ_{Point3}\right|, \ldots, \left|QQ_{267-\beta_1} - QQ_{Point267}\right|$, and respectively define them as $|QQ|_{2-\beta_1}$, $|QQ|_{3-\beta_1}, \ldots,$ $|QQ|_{k-\beta_1}, \ldots, |QQ|_{267-\beta_1}$ $(k = 2, \ldots, 267)$. In order

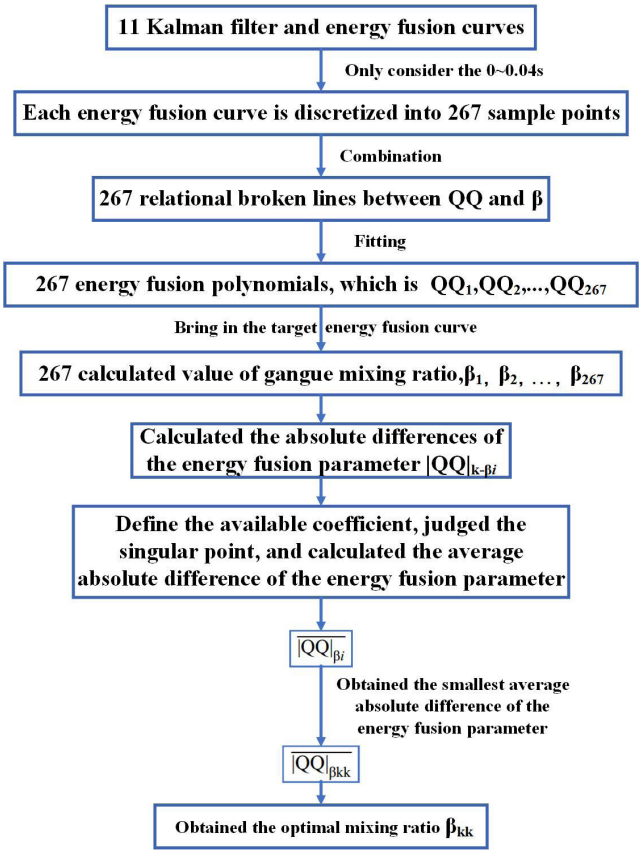

FIGURE 37. Detailed recognition strategy chart.

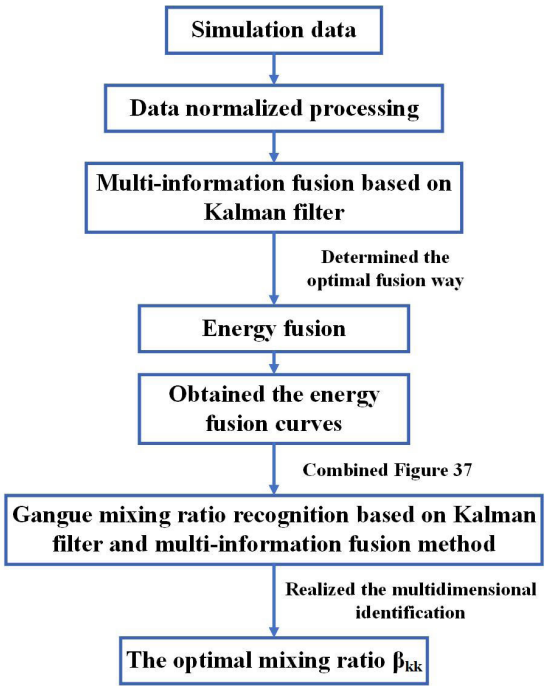

FIGURE 38. Complete recognition flowchart.

to avoid the effect of the singular point to the recognition result, defined the available coefficient of β is ξ, and point k is available when $|QQ|_{k-\beta_1} \leq \xi$. When $|QQ|_{k-\beta_1} > \xi$, the k point is considered as the singular point, then the k^{th} sample point will be deleted. Solving the Mean Value of the absolute differences ($|QQ|_{2-\beta_1}$, $|QQ|_{3-\beta_1}, \ldots, |QQ|_{k-\beta_1}, \ldots, |QQ|_{267-\beta_1}$) of the available point energy fusion parameters in Point 2, Point 3, ..., Point 267 (The sum of absolute differences of available point energy fusion parameters divided by the number of available points), the average absolute difference of its energy fusion parameters was obtained and defined as $\overline{|QQ|_{\beta 1}}$. According to the above process, the calculated value of gangue mixing ratio β_2, $\beta_3, \ldots, \beta_{267}$ and the mean absolute differences of the corresponding energy fusion parameters ($\overline{|QQ|_{\beta 2}}$, $\overline{|QQ|_{\beta 3}}, \ldots \overline{|QQ|_{\beta 267}}$) are obtained respectively.

(4) By comparing $\overline{|QQ|_{\beta 1}}$, $\overline{|QQ|_{\beta 2}}, \ldots, \overline{|QQ|_{\beta 267}}$, the smallest $\overline{|QQ|_{\beta}}$ is obtained and defined as $\overline{|QQ|_{\beta kk}}$, then the corresponding $\beta_{kk}(kk = 1, 2, \ldots, 267)$ is the optimal mixing ratio of the target energy fusion curve.

The principle of the detailed identification strategy for the gangue mixing ratio identification based on Kalman filter and energy fusion is shown in Figure 37. After combining it with the aforementioned signal acquisition and processing method, the recognition flowchart of gangue mixing ratio in this paper is obtained, as shown in Figure 38.

Based on multi-particles impact simulation and Kalman filter, the optimal data fusion processing method is determined to be energy fusion, hereby the recognition strategy of coal gangue mixing ratio is proposed. The recognition strategy is conducted based on the energy fusion function space. In this paper, there are 267 functions in the energy fusion function space, and the minimum mean absolute difference is taken as the evaluation standard to complete the independence and unification of multidimensional parameters, and realized the multidimensional identification. Compared with the coal gangue mixing ratio recognition method based on the multi-time-frequency parameters fusion recognition parameter Q of the acceleration, the recognition rate can be greatly improved and accurate recognition of coal gangue mixing ratio can be effectively realized. At the same time, the applicability of this recognition strategy is very high. It can select the data fusion method, fusion function fitting forms (such as polynomial fitting, nonlinear fitting, exponential fitting, logarithmic fitting, etc.), dimensions of fusion space (267 dimensions are used in this article, which can be increased or decreased depending on the actual data) and judging standard (In this paper, the minimum mean absolute difference is used as the standard.) according to the data form (theoretical, simulation, or test data). By virtue of the idea of the data processing and optimal mixing ratio selecting in the identification strategy, the recognition strategy can be extended to intelligent recognition, intelligent sorting, intelligent optimization and other fields.

VI. CONCLUSION

This paper established the theoretical model when multiple coal gangue particles elastic impacting the metal plate for the first time simultaneously in an undisturbed way, conducted the brittle impact contact simulation between coal gangue and the metal plate. Through the analysis of the system elastic contact force, particles breakage state and the metal plate contact response under different mixed gangue ratios, the influence law of coal gangue volume mixing ratio on the system contact response was obtained. The time-frequency domain characteristics of the metal plate vibration acceleration were analyzed, and the recognition technology of coal gangue mixing ratio based on multi-time-frequency parameters fusion of the metal plate vibration acceleration and the recognition technology based on the multidimensional contact response information fusion of the metal plate were studied respectively. The following conclusions are obtained:

(1) With the increase of gangue mixing ratio, the total maximum elastic contact force between the multi-particles and the metal plate increases. Particles totally broken area, maximum displacement, velocity, acceleration and overall stress value of the metal plate, the total maximum brittle contact force and each part of energy all increase accordingly

(2) With the increase of gangue mixing ratio, the energy characteristic value of each IMF component, mean value, waveform index and kurtosis index of the metal plate vibration acceleration signal show disorderly change. The square root amplitude, absolute mean, variance, peak-to-peak value, root mean square value and marginal spectral energy value show the increasing trend as a whole. The skewness and margin index show the downward trend as a whole.

(3) Based on the basic parameters such as the square root amplitude, absolute mean, variance, peak-to-peak value, root mean square value, marginal spectral energy value, skewness and margin index of the metal plate vibration acceleration, the fusion recognition parameter is put forward and obtained its relation equation. Through analysis, fusion identification parameter Q based on the metal plate acceleration multi-time-frequency parameters are more suitable for the prediction of coal gangue mixing ratio. When the actual gangue mixing ratio is close to the simulation one, there will be a large deviation.

(4) Energy fusion, other response fusion, absolute value fusion of other responses and the composite fusion are carried out through Kalman filter data fusion method based on the metal plate acceleration, velocity, displacement, internal energy, kinetic energy, total energy, absolute value of acceleration, absolute value of velocity and displacement. Research show that the energy fusion mode presents a single peak trend, and the fusion parameter curve has low fluctuation, high stationarity, its stratification and difference are the most significant in the four fusion modes, so it is the optimal fusion processing mode.

(7) Based on Kalman filter and energy fusion, multi-dimensional recognition strategy of optimal gangue mixing

ratio with high recognition accuracy and applicability is proposed.

The conclusions of this paper will provide theoretical and research basis for the study of the impact contact responses between coal gangue and the hydraulic support, provide multi-dimensional accurate recognition strategy for the recognition of coal gangue mixing ratio, and provide reference for the research and realization of coal gangue interface recognition technology in top coal caving.

REFERENCES

[1] A. Vakili and B. K. Hebblewhite, "A new cavability assessment criterion for longwall top coal caving," *Int. J. Rock Mech. Mining Sci.*, vol. 47, no. 8, pp. 1317–1329, Dec. 2010, doi: 10.1016/j.ijrmms.2010.08.010.

[2] N. Zhang, C. Liu, and P. Yang, "Flow of top coal and roof rock and loss of top coal in fully mechanized top coal caving mining of extra thick coal seams," *Arabian J. Geosci.*, vol. 9, no. 6, p. 465, May 2016, doi: 10.1007/s12517-016-2493-8.

[3] J.-W. Zhang, J.-C. Wang, W.-J. Wei, Y. Chen, and Z.-Y. Song, "Experimental and numerical investigation on coal drawing from thick steep seam with longwall top coal caving mining," *Arabian J. Geosci.*, vol. 11, no. 5, p. 96, Mar. 2018, doi: 10.1007/s12517-018-3421-x.

[4] H. Alehossein and B. A. Poulsen, "Stress analysis of longwall top coal caving," *Int. J. Rock Mech. Mining Sci.*, vol. 47, no. 1, pp. 30–41, Jan. 2010, doi: 10.1016/j.ijrmms.2009.07.004.

[5] Q. Zeng, Y. Yang, X. Zhang, L. Wan, J. Zhou, and G. Yin, "Study on metal plate vibration response under coal–gangue impact based on 3D simulation," *Arabian J. Sci. Eng.*, vol. 44, no. 9, pp. 7567–7580, Sep. 2019, doi: 10.1007/s13369-019-03853-3.

[6] Y. Yang, Q. Zeng, and L. Wan, "Dynamic response analysis of the vertical elastic impact of the spherical rock on the metal plate," *Int. J. Solids Struct.*, vol. 158, pp. 287–302, Feb. 2019, doi: 10.1016/j.ijsolstr.2018.09.017.

[7] Y. Yang, Q. Zeng, and L. Wan, "Contact response analysis of vertical impact between elastic sphere and elastic half space," *Shock Vib.*, vol. 2018, Nov. 2018, Art. no. 1802174, doi: 10.1155/2018/1802174.

[8] Y. Yang, Q. Zeng, G. Yin, and L. Wan, "Vibration test of single coal gangue particle directly impacting the metal plate and the study of coal gangue recognition based on vibration signal and stacking integration," *IEEE Access*, vol. 7, pp. 106784–106805, 2019, doi: 10.1109/ACCESS.2019.2932118.

[9] Q. L. Zeng, Z. Y. Xin, Y. Yang, B. Chen, and L. R. Wan, "Stress analysis of the hinge point of hydraulic support of coal gangue granular impact caving coal based on Abaqus," *J. Shandong Univ. Sci. Technol.*, vol. 38, no. 3, pp. 35–42, 2019, doi: 10.16452/j.cnki.sdkjzk.2019.03.004.

[10] Y.-S. Xie and Y.-S. Zhao, "Numerical simulation of the top coal caving process using the discrete element method," *Int. J. Rock Mech. Mining Sci.*, vol. 46, no. 6, pp. 983–991, Sep. 2009, doi: 10.1016/j.ijrmms.2009.03.005.

[11] S. Yang, J. Zhang, Y. Chen, and Z. Song, "Effect of upward angle on the drawing mechanism in longwall top-coal caving mining," *Int. J. Rock Mech. Mining Sci.*, vol. 85, pp. 92–101, May 2016, doi: 10.1016/j.ijrmms.2016.03.004.

[12] S. L. Yang, H. H. Liu, Y. Li, and L. Y. Zheng, "The technology on full mechanized caving with combine-layers in very contiguous seams," *J. China Coal Soc.*, vol. 36, no. 3, pp. 371–376, 2011, doi: 10.13225/j.cnki.jccs.2011.03.016.

[13] J. C. Wang, J. W. Zhang, S. L. Yang, and Z. Y. Song, "3-D movement law of top-coal in near horizontal coal seam with multi-gangue under caving mining technique," *J. China Coal Soc.*, vol. 40, no. 5, pp. 979–987, 2015, doi: 10.13225./j.cnki.jccs.2014.1325.

[14] J. W. Zhang, J. C. Wang, and W. J. Wei, "Effect of face dip angle on the drawing mechanism in longwall top-coal caving mining," *J. China Univ. Mining Technol.*, vol. 47, no. 4, pp. 805–814, 2018, doi: 10.13247/j.cnki.jcumt.000889.

[15] Z. Song and H. Konietzky, "A particle-based numerical investigation on longwall top coal caving mining," *Arabian J. Geosci.*, vol. 12, no. 18, p. 556, Sep. 2019, doi: 10.1007/s12517-019-4743-z.

[16] N. Zhang, C. Liu, X. Wu, and T. Ren, "Dynamic random arching in the flow field of top-coal caving mining," *Energies*, vol. 11, no. 5, p. 1106, May 2018, doi: 10.3390/en11051106.

[17] J. Wang, J. Zhang, Z. Song, and Z. Li, "Three-dimensional experimental study of loose top-coal drawing law for longwall top-coal caving mining technology," *J. Rock Mech. Geotechn. Eng.*, vol. 7, no. 3, pp. 318–326, Jun. 2015, doi: 10.1016/j.jrmge.2015.03.010.

[18] J. W. Zhang, W. D. Pan, Z. L. Li, and Z. Y. Song, "Development and application of 3D simulation test device for loose top-coal drawing under caving mining technique," *Chin. J. Rock Mech. Eng.*, vol. 34, no. 2, pp. 3871–3879, 2015, doi: 10.13722/j.cnki.jrme.2014.0620.

[19] N. Zhang and C. Liu, "Radiation characteristics of natural gamma-ray from coal and gangue for recognition in top coal caving," *Sci. Rep.*, vol. 8, no. 1, p. 190, Dec. 2018, doi: 10.1038/s41598-017-18625-y.

[20] W. Hou, "Identification of coal and gangue by feed-forward neural network based on data analysis," *Int. J. Coal Preparation Utilization*, vol. 39, no. 1, pp. 33–43, Jan. 2019, doi: 10.1080/19392699.2017.1290609.

[21] L. Si, Z. Wang, X. Liu, C. Tan, J. Xu, and K. Zheng, "Multi-sensor data fusion identification for shearer cutting conditions based on parallel quasi-Newton neural networks and the Dempster–Shafer theory," *Sensors*, vol. 15, no. 11, pp. 28772–28795, Nov. 2015, doi: 10.3390/s151128772.

[22] Q. Song, H. Jiang, Q. Song, X. Zhao, and X. Wu, "Combination of minimum enclosing balls classifier with SVM in coal-rock recognition," *PLoS ONE*, vol. 12, no. 9, Sep. 2017, Art. no. e0184834, doi: 10.1371/journal.pone.0184834.

[23] Q. Song, H. Jiang, X. Zhao, and D. Li, "An automatic decision approach to coal-rock recognition in top coal caving based on MF-score," *Pattern Anal. Appl.*, vol. 20, no. 4, pp. 1307–1315, Nov. 2017, doi: 10.1007/s10044-017-0618-7.

[24] J. Sun and B. Su, "Coal–rock interface detection on the basis of image texture features," *Int. J. Mining Sci. Technol.*, vol. 23, no. 5, pp. 681–687, Sep. 2013, doi: 10.1016/j.ijmst.2013.08.011.

[25] D. P. Tripathy and K. Guru Raghavendra Reddy, "Novel methods for separation of gangue from limestone and coal using multispectral and joint color-texture features," *J. Inst. Eng. (India) D*, vol. 98, no. 1, pp. 109–117, Apr. 2017, doi: 10.1007/s40033-015-0106-4.

[26] W. Liu, K. He, C.-Y. Liu, Q. Gao, and Y.-H. Yan, "Coal-gangue interface detection based on Hilbert spectral analysis of vibrations due to rock impacts on a longwall mining machine," *Proc. Inst. Mech. Eng. C, J. Mech. Eng. Sci.*, vol. 229, no. 8, pp. 1523–1531, Jun. 2015, doi: 10.1177/0954406214543409.

[27] D. Dou, D. Zhou, J. Yang, and Y. Zhang, "Coal and gangue recognition under four operating conditions by using image analysis and relief-SVM," *Int. J. Coal Preparation Utilization*, pp. 1–10, Oct. 2018, doi: 10.1080/19392699.2018.1540416.

[28] Z. Wang, L. Si, C. Tan, and X. Liu, "A novel approach for shearer cutting load identification through integration of improved particle swarm optimization and wavelet neural network," *Adv. Mech. Eng.*, vol. 6, Jan. 2014, Art. no. 521629, doi: 10.1155/2014/521629.

[29] X. Y. Cong, Z. C. Wang, B. P. Wang, and W. L. Peng, "Application of filtering method based on EMD and kurtosis in coal-rock interface recognition," *J. Vib., Meas. Diagnosis*. vol. 35, no. 5, pp. 950–954 and 995, 2015, doi: 10.16450/j.cnki.issn.1004-6801.2015.05.024.

[30] X. Wang, "Study of coal-rock identification method based on electromagnetic wave technology," M.S. thesis, School Inf. Control Eng., China Univ. Mining Technol., Jiangsu Sheng, China, 2017.

[31] X. Wang, K.-X. Hu, L. Zhang, X. Yu, and E.-J. Ding, "Characterization and classification of coals and rocks using terahertz time-domain spectroscopy," *J. Infr., Millim., THz Waves*, vol. 38, no. 2, pp. 248–260, Feb. 2017, doi: 10.1007/s10762-016-0317-2.

[32] S. J. Huang, "The coal-rock interface recognition research based on the digital image processing and clustering technology," M.S. thesis, School Mech. Electron. Inf. Eng., China Univ. Mining Technol., Beijing, China, 2016.

[33] W. Hua, X. Zhao, C. Luo, G. Xue, and M. Wu, "Coal-rock interface recognition method based on dimensionless parameters and support vector machine," *Electron. J. Geotech. Eng.*, vol. 21, no. 16, pp. 5477–5486, 2016.

[34] H. Minamoto and S. Kawamura, "Moderately high speed impact of two identical spheres," *Int. J. Impact Eng.*, vol. 38, nos. 2–3, pp. 123–129, Feb. 2011, doi: 10.1016/j.ijimpeng.2010.09.005.

[35] M. R. Brake, "The effect of the contact model on the impact-vibration response of continuous and discrete systems," *J. Sound Vib.*, vol. 332, no. 15, pp. 3849–3878, Jul. 2013, doi: 10.1016/j.jsv.2013.02.003.

[36] C. Thornton, S. J. Cummins, and P. W. Cleary, "On elastic-plastic normal contact force models, with and without adhesion," *Powder Technol.*, vol. 315, pp. 339–346, Jun. 2017, doi: 10.1016/j.powtec.2017.04.008.

[37] Z. Wang, H. Yu, and Q. Wang, "Layer-substrate system with an imperfectly bonded interface: Spring-like condition," *Int. J. Mech. Sci.*, vol. 134, pp. 315–335, Dec. 2017, doi: 10.1016/j.ijmecsci.2017.10.028.
[38] E. Olsson and P.-L. Larsson, "On the tangential contact behavior at elastic-plastic spherical contact problems," *Wear*, vol. 319, nos. 1–2, pp. 110–117, Nov. 2014, doi: 10.1016/j.wear.2014.07.016.
[39] T. Wang, L. Wang, L. Gu, and D. Zheng, "Stress analysis of elastic coated solids in point contact," *Tribology Int.*, vol. 86, pp. 52–61, Jun. 2015, doi: 10.1016/j.triboint.2015.01.013.
[40] R. L. Jackson, I. Green, and D. B. Marghitu, "Predicting the coefficient of restitution of impacting elastic-perfectly plastic spheres," *Nonlinear Dyn.*, vol. 60, no. 3, pp. 217–229, May 2010, doi: 10.1007/s11071-009-9591-z.
[41] K. L. Johnson, *Contact Mechanics*. Cambridge, U.K.: Cambridge Univ. Press, 1985.
[42] S. Krijt, C. Güttler, D. Heißelmann, C. Dominik, and A. G. G. M. Tielens, "Energy dissipation in head-on collisions of spheres," *J. Phys. D, Appl. Phys.*, vol. 46, no. 43, Oct. 2013, Art. no. 435303, doi: 10.1088/0022-3727/46/43/435303.
[43] M. Machado, P. Moreira, P. Flores, and H. M. Lankarani, "Compliant contact force models in multibody dynamics: Evolution of the hertz contact theory," *Mechanism Mach. Theory*, vol. 53, pp. 99–121, Jul. 2012, doi: 10.1016/j.mechmachtheory.2012.02.010.
[44] F. Paulo, M. Margarida, S. Miguel, and M. Jorge, "On the continuous contact force models for soft materials in multibody dynamics," *Multibody Syst. Dyn.* vol. 25, no. 3, pp. 257–375, 2011, doi: 10.1007/s11044-010-9237-4.
[45] L. Skrinjar, J. Slavič, and M. Boltežar, "A review of continuous contact-force models in multibody dynamics," *Int. J. Mech. Sci.*, vol. 145, pp. 171–187, Sep. 2018, doi: 10.1016/j.ijsmecsci.2018.07.010.
[46] A. Sayyad and Y. M. Ghugal, "Bending of shear deformable plates resting on winkler foundations according to trigonometric plate theory," *J. Appl. Comput. Mech.*, vol. 4, no. 3, pp. 187–201, 2018, doi: 10.22055/jacm.2017.23057.1148.
[47] J. C. Monge, J. L. Mantari, J. Yarasca, and R. A. Arciniega, "On bending response of doubly curved laminated composite shells using hybrid refined models," *J. Appl. Comput. Mech.*, vol. 5, no. 5, pp. 875–899, 2019, doi: 10.22055/jacm.2019.27297.1397.
[48] K. Ye, L. Li, and H. Zhu, "A note on the hertz contact model with nonlinear damping for pounding simulation," *Earthq. Eng. Struct. Dyn.*, vol. 38, no. 9, pp. 1135–1142, Jul. 2009, doi: 10.1002/eqe.883.
[49] T. Kalvoda and Y.-R. Hwang, "A cutter tool monitoring in machining process using Hilbert–Huang transform," *Int. J. Mach. Tools Manuf.*, vol. 50, no. 5, pp. 495–501, May 2010, doi: 10.1016/j.ijmachtools.2010.01.006.
[50] H. Zhao, M. Sun, W. Deng, and X. Yang, "A new feature extraction method based on EEMD and multi-scale fuzzy entropy for motor bearing," *Entropy*, vol. 19, no. 1, p. 14, Dec. 2016, doi: 10.3390/e19010014.
[51] J. Cheng, D. Yu, J. Tang, and Y. Yang, "Local rub-impact fault diagnosis of the rotor systems based on EMD," *Mechanism Mach. Theory*, vol. 44, no. 4, pp. 784–791, Apr. 2009, doi: 10.1016/j.mechmachtheory.2008.04.006.
[52] Y. Chen, C.-T. Wu, and H.-L. Liu, "EMD self-adaptive selecting relevant modes algorithm for FBG spectrum signal," *Opt. Fiber Technol.*, vol. 36, pp. 63–67, Jul. 2017, doi: 10.1016/j.yofte.2017.02.008.
[53] L. Lin and F. Chu, "HHT-based AE characteristics of natural fatigue cracks in rotating shafts," *Mech. Syst. Signal Process.*, vol. 26, pp. 181–189, Jan. 2012, doi: 10.1016/j.ymssp.2011.07.017.
[54] E. Elbouchikhi, V. Choqueuse, Y. Amirat, M. E. H. Benbouzid, and S. Turri, "An efficient Hilbert–Huang transform-based bearing faults detection in induction machines," *IEEE Trans. Energy Convers.*, vol. 32, no. 2, pp. 401–413, Jun. 2017, doi: 10.1109/TEC.2017.2661541.
[55] C. Junsheng, Y. Dejie, and Y. Yu, "A fault diagnosis approach for roller bearings based on EMD method and AR model," *Mech. Syst. Signal Process.*, vol. 20, no. 2, pp. 350–362, Feb. 2006, doi: 10.1016/j.ymssp.2004.11.002.
[56] Y. Kopsinis and S. McLaughlin, "Development of EMD-based denoising methods inspired by wavelet thresholding," *IEEE Trans. Signal Process.*, vol. 57, no. 4, pp. 1351–1362, 2009, doi: 10.1109/TSP.2009.2013885.
[57] D. Looney and D. P. Mandic, "Multiscale image fusion using complex extensions of EMD," *IEEE Trans. Signal Process.*, vol. 57, no. 4, pp. 1626–1630, Apr. 2009, doi: 10.1109/TSP.2008.2011836.
[58] J. W. Zhang, X. J. Tan, and P. B. Zheng, "Non-destructive detection of wire rope discontinuities from residual magnetic field images using the Hilbert–Huang transform and compressed sensing," *Sensors*, vol. 17, no. 3, p. 608, 2017, doi: 10.3390/s17030608.
[59] H. Wang, Z. Liu, Y. Song, and X. Lu, "Ensemble EMD-based signal denoising using modified interval thresholding," *IET Signal Process.*, vol. 11, no. 4, pp. 452–461, Jun. 2017, doi: 10.1049/iet-spr.2016.0147.
[60] A. G. Espinosa, J. A. Rosero, J. Cusido, L. Romeral, and J. A. Ortega, "Fault detection by means of Hilbert–Huang transform of the stator current in a PMSM with demagnetization," *IEEE Trans. Energy Convers.*, vol. 25, no. 2, pp. 312–318, Jun. 2010, doi: 10.1109/TEC.2009.2037922.
[61] P. Liu, W. Huang, W. Zhang, and F. Li, "An EMD-SG algorithm for spectral noise reduction of FBG-FP static strain sensor," *IEEE Photon. Technol. Lett.*, vol. 29, no. 10, pp. 814–817, May 15, 2017, doi: 10.1109/LPT.2017.2686452.
[62] A.-O. Boudraa and J.-C. Cexus, "EMD-based signal filtering," *IEEE Trans. Instrum. Meas.*, vol. 56, no. 6, pp. 2196–2202, Dec. 2007, doi: 10.1109/tim.2007.907967.
[63] P. Shrivastava, T. K. Soon, M. Y. I. B. Idris, and S. Mekhilef, "Overview of model-based online state-of-charge estimation using Kalman filter family for lithium-ion batteries," *Renew. Sustain. Energy Rev.*, vol. 113, Oct. 2019, Art. no. 109233, doi: 10.1016/j.rser.2019.06.040.
[64] K. Soal, Y. Govers, J. Bienert, and A. Bekker, "System identification and tracking using a statistical model and a Kalman filter," *Mech. Syst. Signal Process.*, vol. 133, Nov. 2019, Art. no. 106127, doi: 10.1016/j.ymssp.2019.05.011.
[65] S. Wen, H. Qi, Z.-T. Niu, Y.-T. Ren, and L.-M. Ruan, "Fast non-intrusive estimation of liquid-phase interface and boundary heat flux in participating media by the Kalman filtering methods," *Int. J. Heat Mass Transf.*, vol. 142, Oct. 2019, Art. no. 118418, doi: 10.1016/j.ijheatmasstransfer.2019.07.068.
[66] J. Y. Lu and X. Li, "Robot indoor location modeling and simulation based on Kalman filtering," *EURASIP J. Wireless Commun. Netw.*, vol. 2019, no. 1, p. 140, Dec. 2019, doi: 10.1186/s13638-019-1462-9.
[67] H. M. Al-Hamadi and K. M. EL-Naggar, "Measurement of synchronous machine parameters using Kalman filter based fuzzy logic estimator," *Measurement*, vol. 43, no. 10, pp. 1327–1335, Dec. 2010, doi: 10.1016/j.measurement.2010.07.012.

YANG YANG received the B.E. degree in machine design and automation from the Shandong University of Science and Technology, in 2015, where he is currently pursuing the Ph.D. degree. His research interests include contact mechanics, coal gangue interface recognition, signal processing, artificial intelligence, mechanical design electromechanical integration, and intelligent control.

QINGLIANG ZENG received the Ph.D. degree in machine design and theory from the China University of Mining and Technology, in 2000. He is currently a Professor with the Shandong University of Science and Technology and Shandong Normal University. He has participated more than 40 projects funded by the National Sci-Tech Support Plan, the National 863 Program, and the Natural Science Foundation of China. He has published more than 90 articles as the principle person. His research interests include electromechanical integration, condition monitoring and fault diagnosis, and virtual prototype.

LIRONG WAN received the Ph.D. degree from the Shandong University of Science and Technology, in 2008. She is currently a Professor with the Shandong University of Science and Technology. Her research interests include virtual prototype, concurrent engineering, computer integrated manufacturing, electromechanical integration, and hydraulic transmission and control.

GUANGJUN YIN received the B.E. degree in machine design and automation and the master's degree from the Shandong University of Science and Technology, in 2016 and 2019, respectively.